DTIC FILE COPY

(2)

AD-A216 969

RITY CLASSIFICATION OF THIS PAGE

REPORT DOCUMENTATION PAGE

Form Approved
OMB No 0704-0188

EPORT SECURITY CLASSIFICATION	1b. RESTRICTIVE MARKINGS
CURITY CLASSIFICATION AUTHORITY	3 DISTRIBUTION / AVAILABILITY OF REPORT Aporoved for public release; distribution unlimited.
CLASSIFICATION / DOWNGRADING SCHEDULE Unclassified	
FORMING ORGANIZATION REPORT NUMBER(S) N00014-79-C-0647	5. MONITORING ORGANIZATION REPORT NUMBER(S)
ME OF PERFORMING ORGANIZATION: Colorado State University 6b OFFICE SYMBOL (If applicable)	7a. NAME OF MONITORING ORGANIZATION
RESS (City, State, and ZIP Code) Department of Chemistry Fort Collins, CO 80523	7b ADDRESS (City, State, and ZIP Code)
8a NAME OF FUNDING / SPONSORING ORGANIZATION: Office of Naval Research 8b. OFFICE SYMBOL (If applicable)	9 PROCUREMENT INSTRUMENT IDENTIFICATION NUMBER N00014-79-C-0647
8c. ADDRESS (City, State, and ZIP Code) 800 North Quincy Street Arlington, VA 22217-5000	10 SOURCE OF FUNDING NUMBERS PROGRAM ELEMENT NO / PROJECT NO / TASK NO / WORK UNIT ACCESSION NO

11 TITLE (Include Security Classification)
"Low Temperature Elastic and Dielectric Properties of Incommensurate Barium Sodium Niobate"

12 PERSONAL AUTHOR(S)
W. F. Oliver, J. F. Scott, R. Nowak and E. R. Bernstein

13a TYPE OF REPORT	13b TIME COVERED	14 DATE OF REPORT (Year, Month, Day)	15 PAGE COUNT
Technical Report	FROM _____ TO _____	December 151989	

16 SUPPLEMENTARY NOTATION

17 COSATI CODES			18 SUBJECT TERMS (Continue on reverse if necessary and identify by block number)
FIELD	GROUP	SUB-GROUP	dielectric properties, Brillouin, birefringence, x-ray crystallography, neutron crystallography, phase transition Barrium sodium niobate, incommensurate phases

19 ABSTRACT (Continue on reverse if necessary and identify by block number)

SEE ATTACHED ABSTRACT

DTIC
ELECTE
JAN 25 1990
S B D

90 01 24 023

20 DISTRIBUTION / AVAILABILITY OF ABSTRACT	21 ABSTRACT SECURITY CLASSIFICATION
☒ UNCLASSIFIED/UNLIMITED ☐ SAME AS RPT ☐ DTIC USERS	Unclassified
22a NAME OF RESPONSIBLE INDIVIDUAL: Elliot R. Bernstein	22b TELEPHONE (Include Area Code): (303) 491-6347 / 22c OFFICE SYMBOL

DD Form 1473, JUN 86 — Previous editions are obsolete. — SECURITY CLASSIFICATION OF THIS PAGE

S/N 0102-LF-014-6603

OFFICE OF NAVAL RESEARCH

Contract N00014-79-C-0647

TECHNICAL REPORT #64

"Low Temperature Elastic and Dielectric Properties of Incommensurate Barium Sodium Niobate"

by

W. F. Oliver, J. F. Scott, R. Nowak and E. R. Bernstein

Submitted for publication in Journal Ferroelectrics

Department of Chemistry
Colorado State University
Fort Collins, Colorado 80523

December 15, 1989

LOW TEMPERATURE ELASTIC AND DIELECTRIC PROPERTIES OF INCOMMENSURATE BARIUM SODIUM NIOBATE

W. F. Oliver* and J. F. Scott

Department of Physics, University of Colorado, Boulder, CO 80309-0390

and

R. Novak† and E. R. Bernstein

Department of Chemistry, Colorado State University, Fort Collins, CO 80523

ABSTRACT

We have performed dielectric and Brillouin spectroscopic measurements on incommensurate (IC) $Ba_2NaNb_5O_{15}$ from ca. 15 K to room temperature and have related our measurements to earlier studies of birefringence and x-ray and neutron crystallography, with special emphasis upon the structural phase transitions near 105 K and 40 K. The 105 K transition is from $Ccm2_1$ to a modulated structure, which appears to be a reentrant phase also found at atmospheric pressure from 565 K to 582 K. Such a reentrant IC/C/IC sequence is predicted in the phenomenological theory of Ishibashi. The lock-in phase below 40 K is tetragonal and probably of space group $P4nc$ (structural refinements of preliminary neutron scattering data are in progress).

* Present address: Department of Physics, Arizona State University, Tempe, AZ 85287. † Present address: —

Acknowledgments: Work at University of Colorado was supported in part by NSF grant DMR86-0666; and at Colorado State University by —.

INTRODUCTION

Barium sodium niobate $Ba_2NaNb_5O_{15}$ (BSN) has been studied extensively over the past twenty years. Initially, it was grown and studied for its nonlinear optical properties.[1-3] In addition to having excellent nonlinear optical properties BSN possesses a sequence of four or more phase transitions that exhibit several features of much current interest to condensed matter scientist. These phase transitions have been the subject of most of the work in BSN over the past fifteen years. Figure 1a shows a schematic illustration of the different phases in BSN as a function of temperature, as well as the point-group symmetries, lattice constants and relative orientations of the a and b axes.[4] This schematic phase diagram represents the understanding of the different phases of BSN at the beginning of this work. Most of the work to date has been done at temperatures above room temperature, particularly in the region of the incommensurate (IC) phase between ~ 543 K and ~ 582 K.[5-20] A new phase diagram is also given in Fig. 1b, which shows our current understanding of the phases of BSN as a function of temperature, as well as a hypothetical pressure dependence. In the present work we will present Brillouin light scattering results and dielectric measurements in the temperature region between ~ 18 K and 300 K.

The first structural analysis of BSN was done by Jamieson *et al.* using x-ray diffraction techniques, and it was found to be of the tetragonal tungsten bronze structure.[21] Above ~ 838 K BSN is in an undistorted, centrosymmetric, paraelectric phase of point-group symmetry 4/mmm. At T_C ~ 838 K, it undergoes a ferroelectric phase transition to a tetragonal polar phase with 4mm symmetry. BSN retains its ferroelectricity throughout all of the lower temperature phases. As the temperature is lowered further another phase transition is encountered at T_I = 582 K. This transition is a displacive ferroelastic transition to an IC phase with an average

orthorhombic point-group symmetry mm2. The orthorhombic a_o and b_o axes occur at 45° with respect to the higher temperature tetragonal a_t and b_t axes, and the IC modulation lies along a_o with an IC k-vector given by

$$\underset{\sim}{k}_I = (1+\delta)\left(\frac{\underset{\sim}{a}_t^* + \underset{\sim}{b}_t^*}{4}\right) + \frac{\underset{\sim}{c}_t^*}{2}. \qquad (1)$$

A nearly complete lock-in transition then occurs at $\sim$ 543 K to a phase with the orthorhombic symmetry. This phase does not stabilize in a perfect commensurate structure due to pinning of discommensurations (DC) or anti-phase boundaries (APB) by defects. The phase below 543 K is thus often referred to as the quasi-commensurate (QC) phase. Pinned APB in the QC phase have been directly observed by a number of groups.[22-24] At $\sim$ 100 K the higher symmetry tetragonal 4mm structure is restored in another phase transition involving the onset of a 2q IC structure, with the directions of the modulations being those of the orthorhombic a_o and b_o directions.[25] Finally, evidence exists for yet another transition between about 10 K and 40 K.[4, 26]

LOW TEMPERATURE PHASE TRANSITIONS

The low temperature properties of BSN are the least studied, and hence, the most enigmatic. Evidence for a phase transition at low temperature first came from an observation of ferroelastic twin domains in a (001) plate, between crossed polarizers.[27] As the sample was cooled, these twins were observed to disappear at about (110±5 K). A similar disappearance of the twin domains can be observed by heating the crystal through T_I, to the tetragonal phase. X-ray and several other physical measurements were then performed to elucidate the nature of this observation.

The difference in the lattice constants $b_o - a_o$ was measured between room temperature and 80 K, using a horizontal x-ray diffractometer.[27] Birefringence (Δn_{ab})

measurements, on a (001) plate from the sample, were also performed over the same temperature range. Both Δn_{ab} and $(b-a)/a$ were found to increase slightly to a maximum at ~250 K, and then to drop off sharply to zero at a temperature near 110±5 K. Thus, unequivocal evidence that BSN undergoes another phase transition near 110 K, to a phase of tetragonal symmetry, was obtained. This transition was found to involve only slight displacements, since x-ray Laue photos taken along [001], at both room temperature and 80 K, yielded identical results, indicating the persistence of the tungsten bronze structure below 110 K. Furthermore, spontaneous polarization (P_S) measurements along [001], and dielectric measurements along [100] and [001] were performed. P_S and ϵ_c were nearly flat between room temperature and 80 K, while ϵ_a showed a monotonic increase on cooling, except for a small anomaly in the 100–130 K temperature region. A finite P_S below 110 K requires a polar tetragonal structure, and the $4mm$ point group symmetry was thus confirmed.

Convincing group theoretical arguments were also put forth[27] to suggest that the phase below $T \sim 110$ K had the same space group symmetry ($P4bm$) as the higher temperature normal phase. Thus, BSN was found to possess an orthorhombic ($mm2$) ferroelastic phase, sandwiched between two paraelastic phases of the same higher tetragonal ($4mm$) point group symmetry (and possibly of the same space group symmetry). This reentrant phenomenon, where a crystal transforms from a higher to a lower symmetry phase, and then back to the same higher symmetry phase upon cooling, is quiet unusual. The only known example among ferroelectrics is Rochelle salt, ironically the first ferroelectric ever discovered.[28] Only a single ferroelastic, the solid solution $Tb_xGd_{1-x}VO_4$, was known to possess this property.[29] In both of these crystals, the stability range of the lower symmetry intermediate phase is very narrow (42 K for Rochelle salt, and 6 K for $Tb_xGd_{1-x}VO_4$), and

thus, BSN is unique in that its reentrant behavior occurs from an intermediate phase which is stable over 470 K at atmospheric pressure.

A subsequent series of similar experiments were then performed by Schneck and Paquet on a variety of BSN samples obtained from different sources.[26] In this paper it was found that only one of five samples studied possessed the phase transition at ~ 110 K. The other samples all showed a significant decrease in the birefringence from about ~ 250 K to ~ 100 K, and then a levelling off of Δn_{ab} at a finite nonzero value. Furthermore, only the sample with a zero birefringence below 100 K produced a dielectric anomaly in ϵ_a near 130 K. They attributed this significant sample variation to differences in stoichiometry. Another paper[30] specifically addressed this problem. Samples of many different solid solutions of $Ba_{2+x}Na_{1-2x}Nb_5O_{15}$ were grown and studied. It was found that the low temperature transition occurred only for crystals grown with a sodium content in the melt, higher than the stoichiometric composition. Since BSN tends to be sodium deficient, this result suggests that the low temperature transition occurs only in samples closest to the pure stoichiometry.

Another interesting anomaly observed by Schneck and Paquet[26] was that the dielectric constant ϵ_a for each sample reached a maximum in the vicinity of 10–20 K, and then showed a slight decrease as the temperature was decreased to 4 K. This anomaly was observed in each sample, regardless of whether the reentrant transition was present. The continuous increase in ϵ_a, between room temperature and 4 K, was also found to be consistent with a continuous softening of a low frequency $B_2(y)$ Raman mode (through the Lyddane-Sachs-Teller relation), reported by Boudou and Sapriel.[10] They thus, hypothesized yet another phase transition from $P4bm$ to either $P4_2bc$ or $P4nc$ for crystals with the reentrant behavior, and from the orthorhombic $Ccm2_1$ to Bb for other samples.

Low temperature Brillouin studies of BSN appear only in the Ph.D. thesis of Jacques Schneck.[31] These data show a tendency for the difference in the elastic

constants $c_{22} - c_{11}$ to become smaller as the temperature is lowered, consistent with an approach to a tetragonal phase. However, the BSN sample used in this experiment had a large number of ferroelastic domains, making it difficult to independently measure the temperature dependence of c_{11} and c_{22}. In general, the data are incomplete and of lower quality than his other measurements of the low temperature properties of BSN. The elastic constant c_{22} could only be measured down to $\sim$ 170 K, and even then the scatter in the data was quite large. As a result, he passed the laser beam emerging from the crystal back through with a spherical mirror, and simultaneously measured both the [100] and [010] LA phonons, in the different domains. At room temperature, the elastic anisotropy of these two modes is about 1 GHz, and so a broad two-peaked convolution of the two phonons appeared in the spectrum. This feature approached a single symmetric Lorentzian at $\sim$ 110 K; evidence of the tetragonal phase.

Finally, neutron and x-ray scattering experiments were performed to probe the low temperature properties of BSN.[25] X-ray precession photos were taken in the (001/2) reciprocal-space plane and they revealed not only the quasi-commensurate satellites with wave-vector $\underset{\sim}{k}_I$ [Eq. (1)], but also, the onset of a new set of satellites around points with wavevector

$$\underset{\sim}{k}_I' = (1+\delta)\left(\frac{\underset{\sim}{a}_t^* - \underset{\sim}{b}_t^*}{4}\right) + \frac{\underset{\sim}{c}_t^*}{2}. \qquad (2)$$

In the tetragonal phase, these wavevectors belong to the same star of k-vectors as $\underset{\sim}{k}_I$, and lie along the other diagonal direction, i.e., along b_o. The actual scattering had the shape of diffuse rods parallel to a_o, with a maximum intensity at $\underset{\sim}{k}_I'$. These rods are similar (though perpendicular) to rods observed above T_I, as precursor effects to the high temperature IC phase. However, these low temperature rods were never observed to condense into sharp satellites at any temperature, down to 4 K. Inelastic neutron scattering confirmed these results. No soft phonon was

detected near the 110 K transition, however, a low frequency branch with limited softening was found at $\sim$ 250 K. Scans perpendicular to the rods along $\underset{\sim}{k}_I'$, show the same linewidth at 20 K and at room temperature, with a broad maximum at $\sim$ 210 K.

One possible explanation of these observations involves the hypothesis of a transition to a tetragonal phase, induced by the onset of a second IC modulation at $\underset{\sim}{k}_I'$, perpendicular to that at $\underset{\sim}{k}_I$. Another interpretation involves a symmetry and phenomenological treatment in which higher terms, i. e., those proportional to the eighth power of the order parameter, are kept in the Landau free energy expansion. Both of these interpretations fail to account for all of the low temperature observations, and thus, the nature of BSN at low temperatures remains unclear.[25]

BRILLOUIN SCATTERING EXPERIMENT

Two samples were cut from the same parent sample of BSN. One of these (sample I) was then prepared so that its faces were oriented along the orthorhombic $a_o - b_o - c_o$ axes. It had dimensions of 2.5 $\times$ 3.9 $\times$ 4.3 mm. The other (sample II) had dimensions of 1.2 $\times$ 1.2 $\times$ 3.8 mm and was oriented with its faces along the tetragonal axes. Precession and back-Laue x-ray diffraction techniques were used for orienting the samples. Both samples were ferroelectrically poled by heating them to a temperature near T_C in a water vapor atmosphere, applying an electric field of about 300 V/cm, and then cooling them slowly while maintaining the field. Furthermore, both samples were heated again to a temperature near T_I and then slowly cooled in the presence of a uniaxial stress field of about 1000 dynes/cm^2, in order to remove ferroelastic twin domains. The direction of the stress defined the orthorhombic a_o axis. This produced two samples that were single domain both ferroelectrically and ferroelastically. Finally, both samples were ground and

polished to have an optical finish. It should be pointed out that some of the important details of the sample preparation techniques have been omitted here. For a more detailed discussion see reference 4.

The basic Brillouin scattering apparatus used in this work has been described in earlier work.[32] A schematic diagram of the optical and data acquisition system is given in Fig. 2. Laser excitation at a wavelength of 5145 Å was provided by a Spectra Physics model 165 argon-ion laser. Typical laser powers used during the experiments were in the 200–350 mW range. An intra-cavity etalon was used for single mode operation of the laser. The long focal length lens L1 focused the incident laser light into the sample. Scattered light was collected at an angle of 90° from the incident direction by lens L2 and then spatially filtered, collimated, and expanded by lens L3, pinhole P1, and lens L4. Just before pinhole P1 a small filter mounted to a relay switch was placed. This filter was triggered to enter the light path during the Rayleigh part of the scan, thus enabling us to use higher laser intensities without causing damage to the PMT. After passing the spatial filter just described, the collimated beam is then analyzed by a Fabry-Perot interferometer (FPI).

The interferometer used in these experiments is a triple-pass piezoelectrically scanned Fabry-Perot purchased from Burleigh. Its plane-mirror etalon consisted of Burleigh mirrors flat to $\lambda/200$ and with a reflectivity of $\sim$ 80 %. Retro reflectors allowed the beam to be passed through the Fabry-Perot three times. The whole interferometer was enclosed in a temperature controlled box and maintained at a temperature of $\sim$ 35° C. A free spectral range of 31.70 GHz was used throughout the experiment and a finesse of $\sim$ 45 was typically obtained.

Next the transmitted beam was focused by lens L5 through pinhole P2 and onto the photocathode of an RCA C31034-02 photomultiplier tube (PMT). By thermoelectrically cooling the PMT to −20° C a dark count of about 10 s^{-1} was

maintained. Photon counting and data acquisition and stabilization were performed with a Burleigh DAS-1, the output of which was stored by a Nicolet 1074 multichannel analyzer (MCA). The MCA was controlled by an IBM XT computer via a GPIO 16 bit parallel interface built on a JDR Microdevices board and plugged directly into the computer. Spectra were plotted on an x-y recorder and digitally stored on floppy disk for further analysis. Phonon frequency shifts for both the longitudinal and transverse acoustic (LA and TA) modes were measured to $\sim \pm 0.25\%$ and the phonon halfwidths to $\sim \pm 3.0\%$.

Samples were affixed to a small copper block using G. E. 7031 varnish and the block was then mounted in a copper scattering cell wrapped with heater wire. This cell was attached to the secondary cold stage of a CTI model 21 closed cycle helium refrigerator, which was used to obtain temperatures as low as 18 K. The temperature was controlled to within ± 0.1 K, using a silicon diode sensor and a proportional temperature controller built at Colorado State University. Another calibrated Si diode monitored by the same temperature controller was used to measure the sample temperature.

Brillouin scattering measurements of the LA and TA modes propagating along the orthorhombic a_o and b_o axes were performed. The LA and TA phonon modes propagating along the a_o axis correspond to the c_{11} and c_{55} elastic constants, respectively, whereas the LA and TA modes along the b_o axis correspond to c_{22} and c_{44}, respectively.[33] All of these modes were measured over the temperature range between room temperature and $\sim$ 50 K. A single data point was obtained at 18 K, but the uncertainties of this point are much larger than those of the others. For each propagation direction, both the LA and TA modes were simultaneously measured by choosing an appropriate FSR. Measurements were also made of the acoustic modes propagating along the orthorhombic $a_o - b_o$ diagonal axes, which do not correspond to pure elastic constants, but rather a mixture of pure constants. These

modes do however correspond to pure modes in the low temperature tetragonal phase. The elastic constant c_{66}, corresponding to the spontaneous shear strain is invisible to Brillouin scattering for the point group symmetries of BSN,[34] however this mode does contribute to the phonon frequencies measured along the diagonals. Table 1 gives a listing of the observed phonon modes for the different scattering geometries used in these experiments.

Figures 3 and 4 show a typical spectrum near room temperature and near the low temperature phase transition, respectively. Note the decrease in intensity of the low temperature phonons and the overall small scattering cross section for phonon modes in BSN. Longer scan times are required at low temperatures and the Airy function background becomes much more apparent. This background makes a determination of the true phonon frequency shifts and widths more difficult. To circumvent this problem, the background of the spectra were fit with a cubed (n=3) Airy function[35]

$$T_n \approx \left[\left(1 - \frac{A}{1-R}\right)^2 \frac{1}{1 + \frac{4R}{(1-R)^2}\sin^2\frac{4\pi L}{\lambda_i}}\right]^n, \qquad (3)$$

where T, R and A are the fractions of the incident light that are transmitted, reflected and absorbed at each surface, respectively, L is the spacing between the Fabry-Perot mirrors, and λ_i is the incident laser wavelength. The value of n in this expression corresponds to the number of times the scattered light is passed through the Fabry-Perot, which is three in our case. These fits were then subtracted from the raw spectra. Fitting was done with a nonlinear least squares program based on the Marquardt method.[36, 37]

An approximation to Eq. (3), which is good near a Fabry-Perot transmission maximum, can be derived by expanding the denominator in a Taylor series expansion. Keeping only the lowest term and rewriting the argument of the sine function

in terms of frequency, the Airy function of Eq. (3) can be approximated by an instrumental function of the form

$$I(\omega) = \frac{A'}{[1 + \alpha^2(\omega - \omega_0)^2]^n} + B, \tag{4}$$

where A' is the strength of the interference maximum, B is the background, n is the number of passes of the interferometer, α is proportional to the width, and ω_0 is the frequency at which the maximum occurs. Equation (4) is also a good approximation to the phonon lineshape for underdamped phonons measured by a single-pass Fabry-Perot (with n=1), and with a small correction factor to those measured by a triple-pass system.[38] After subtracting off the Airy function background, the LA and TA phonons were then fit using Eq. (4), with n=3. Excellent fits were obtained indicating that Eq. (4) adequately describes the phonon lineshapes obtained in this experiment. Brillouin frequency shifts obtained from these fits can then be converted to sound velocities using the relationship[39]

$$\nu_{ph} = \pm\frac{v_{ph}}{\lambda_L}[(\eta_I - \eta_S)^2 + 4\eta_I\eta_S \sin^2(\theta/2)]^{\frac{1}{2}}, \tag{5}$$

where ν_{ph} and v_{ph} are the phonon frequency and sound velocity, λ_L is the laser wavelength, η_I and η_S are the indices of refraction for the incident and scattered light, and θ is the scattering angle. For a scattering angle of 90°, Eq. (5) simpifies to

$$\nu_{ph} = \pm\frac{v_{ph}}{\lambda_L}(\eta_I^2 + \eta_S^2)^{\frac{1}{2}}. \tag{6}$$

Finally, elastic constants can be determined from the sound velocities through the relation $c = \rho v^2$, where ρ is the mass density. The exact relationships between the v_{ij} and c_{ij} measured in our experiments are given in Table 2.

Figure 5 shows the temperature dependence of the LA modes associated with the c_{11} and c_{22} elastic constants, and the TA modes associated with c_{55} and c_{44}.

The elastic constant c_{22} shows a fairly flat temperature dependence with a small dip near T_I' =105 K, whereas c_{11} continuously increases between room temperature and ~ 110 K. Below ~ 95 K the two elastic constants are equal in value, as expected in the tetragonal symmetry. These data were all taken as the sample was cooled and represent more than one cooling run for each crystal direction. On at least one particular cooling run for each direction, careful attention was paid to the temperature region near 105 K. Spectra were obtained in a continuous sequence, each separated by a small temperature from the previous one. During one of these runs a small anomaly of < 1% was observed in the c_{11} data and no anomaly was observed in the c_{22} data other than the dip already mentioned. A subsequent run was not able to reproduce completely the c_{11} anomaly at 105 K. There was no observed anomaly in the phonon halfwidths over the temperature range studied.

The TA modes associated with c_{44} and c_{55} were nearly identical in value. They showed a slight increase of ~ 0.2 GHz as the temperature was lowered from room temperature to ~ 50 K. A small step-like anomaly of about 0.1 GHz was observed at 105 K. This anomaly was more pronounced in the c_{44} data. Finally, the quasi-longitudinal and quasi-transverse acoustic modes measured along the orthorhombic diagonals behaved qualitatively like c_{11} and c_{55}, indicating that the four pure modes already discussed make the dominant contribution to these diagonal modes (see Table 2 and Fig. 6).

OPTICAL DAMAGE

It became exceeding difficult to do Brillouin spectroscopy at temperatures lower than about 80 K. In addition to the fact that the scattering cross section becomes smaller at these temperatures, another problem was encountered. The elastic scattering by the sample increased significantly. At room temperature the beam

of laser light transmitted through the sample created a circular spot of light on the wall of the lab. This wall was about a meter from the sample and the circular spot had a diameter of $\sim$ 2 cm. Below $\sim$ 200 K the equilibrium spot was much larger in size and more complicated in structure. For temperatures near 100 K this spot became as large as 20–25 cm and was observed to have different regions of fluctuating intensity with fluctuations on time scales of seconds. Furthermore, elastic scattering at 90° increased making it difficult to keep from saturating the PMT even with the filter in during the Rayleigh part of the ramp.

Another interesting feature of this strong low temperature scattering was observed when the sample (and refrigerator) were translated by a small amount with respect to the incident laser beam. Immediately after such a translation the transmitted laser beam would again form a small pure spot on the lab wall. Soon after the translation was over however, this spot was observed to deteriorate or relax into the large area equilibrium spot described above. As the temperature was lowered the time of relaxation decreased and the equilibrium spot size grew. For temperatures below $\sim$ 100 K a quick translation resulted in an almost immediate deterioration of the laser spot.

After observing this effect for some time and at several different positions in the crystal, we blocked the incident laser and passed white light through the refrigerator windows. The different paths through which the laser had passed were clearly visible in the crystal. A permanent (or at least metastable) modification of the local index of refraction had occurred. Optically, the crystal had become damaged by the presence of a focused laser beam at low temperatures. The optically damaged BSN crystal was then observed to self-anneal at room temperature. Only a few minutes ($\sim$ 15 to 20) after removal from the cryogenic refrigerator the sample was optically clear, showing no sign of the damage. This optical damage seemed to be more pronounced when the propagation direction of the laser was along the

orthorhombic a_o or b_o axis, than when it was along the 45° bisectors of these axes, i.e., along the tetragonal a_t or b_t axes.

An explanation of this optical damage phenomenon lies in the fact that BSN is a photorefractive material. Its photorefractive tensor elements were measured by Geusic *et al.*[2] and by Singh *et al.*[6] and r_{i3}, for i=1–3, were found to be rather large (the stress free electro-optic coefficients r_{13}^T, r_{23}^T, and r_{33}^T have values of 15, 13, and $48 \times 10^{12}\, m/V$, respectively). Photorefractivity in BSN has its origins in the linear (or Pockels) electro-optic effect. This effect is commonly described in terms of the third-rank linear electro-optic tensor $r_{ij,k}$ defined by the expression

$$\Delta\left(\frac{1}{n^2}\right)_{ij} = \sum_k r_{ij,k} E_k, \tag{7}$$

where n is the index of refraction and E is an electric field. The tensor $r_{ij,k}$ is symmetric under interchange of the indices i and j. Normally, these two indices are contracted (Voight notation) and the r-tensor is written with two indices. From Eq. (7) we see that the optical indicatrix[40] is altered by an electric field in the linear electro-optic effect.

The origin of this time-dependent photorefractive effect in BSN is thought to be similar to that in lithium niobate.[41–44] In this class of electro-optic materials, mobile charges are excited in the presence of a laser and migrate away from the regions of high laser intensity. This builds up large static space-charge fields which couple to the index of refraction through the electro-optic coefficients via Eq. (7). There is a competition between a laser driving force, which tends to push these charges out of the region of the laser, and the tendency for the charges to be randomized by thermal diffusion. At low temperatures in BSN the thermal diffusion is too low to compete successfully and the migrant charges move, altering the optical properties of the crystal. Self annealing occurs at room temperature when the space-charge fields relax as the charges become thermally randomized. Oliver and Scott[45] have

suggested a way in which this effect might be used to gain more information about diffusion in the IC phase of BSN.

DIELECTRIC MEASUREMENTS

Since our particular BSN crystals show the rather uncommon reentrant transition and since Brillouin experiments were not possible near 12 K, we performed dielectric measurements at low temperatures. Small capacitor plates ($\sim 5 \times 5$ mm) with guard rings were made using standard printed circuit techniques. A sample was placed between the capacitor plates and attached with a smooth coating of silver paint. A metal plate with a vacuum tight electrical feedthrough was machined. This plate replaced one of the windows of the CTI closed cycle helium refrigerator. The capacitor plates with the sample was then placed into the copper scattering cell attached to the lower cold stage of the refrigerator. Thermal grease insured good thermal contact. Tiny wires connected the capacitor plates and the guard rings to the electrical feedthroughs. Short coaxial cable connected the outside of the feedthroughs to a Tektronix Model 130 LC meter. Temperature control was achieved with the identical system used with the Brillouin apparatus, described above.

The combined capacitance of the cables, feedthroughs, and capacitor plates was measured before placing the crystal between the plates. This value was then zeroed in an attempt to obtain the capacitance of the sample only. Next the sample capacitance was offset by a constant amount so that the most sensitive scale ($3\,pF$ full scale) of the LC meter could be used. All measurements were done at 120 kHz with a maximum of $1\,V$ across the sample. An accuracy of 3% of the full scale is given in the specifications of the LC meter.

Measurements were made between room temperature and $\sim$ 17 K, which is the lower limit of the closed cycle helium refrigerator with a sample inside. A small time was allowed at each temperature for equilibrium to be established before recording the capacitance. Equilibrium was determined when no further changes were observed in the capacitance. Each data run consisted of a slow cooling followed by a slow heating back to room temperature. At least two data runs were performed for each crystal direction. Capacitance vs. temperature data were also recorded for the empty capacitor plates with a plate separation equal to the crystal thickness. These data were then subtracted from the crystal data to correct for the temperature dependence of the capacitor itself.

Capacitances were converted to dielectric constant using the simple relation

$$\kappa \equiv \frac{\epsilon}{\epsilon_0} = \frac{d}{A\epsilon_0} C, \tag{8}$$

where d is the sample height, A is the area of the sample in contact with the plates, and ϵ_0 is the permittivity of the vacuum. Figure 7 shows the temperature dependences of the dielectric constants κ_a and κ_b measured along the orthorhombic axes. Relative capacitance vs. temperature measurements were extremely reliable since the LC meter showed only smooth continuous changes. There is however, some uncertainty in the absolute capacitance values resulting from the exact value of C for the cables and electrical feedthroughs. A small uniform shift was needed to cause the data for the two crystal directions to overlap at $\sim$ 130 K.

At room temperature $\kappa_a \sim 222 \pm 5$ and $\kappa_b \sim 248 \pm 5$. This difference, which is a measure of the anisotropy in the orthorhombic phase, is similar to previously reported values.[6] Qualitatively, our data are similar in most respects to those of Schneck *et al.*[27] and Schneck and Paquet.[26] The small anomaly at $\sim$ 130 K in the κ_a and κ_b data is in excellent agreement with the earlier data, as are the overall

values of κ between room temperature and 20 K. Unlike the CNET group, however, we observe a clear anomaly in the 30–50 K region.

Another interesting feature of the dielectric data is the fact that κ_a and κ_b do not overlap in the tetragonal phase. In fact, we were never able to obtain data which overlapped in the temperature region between about 25–30 K and ~ 130 K. Furthermore, when the cooling and heating data from a single data run is compared, this same thermal hysteresis is observed. Figure 8 shows an example of this phenomenon for a cooling and heating run along the a_o axis.

DISCUSSION OF THE LOW TEMPERATURE RESULTS

Though a stoichiometric analysis of our samples has not been performed, it is clear that they are of the proper stoichiometry to possess the reentrant tetragonal phase. This is most clearly demonstrated by the temperature dependences of the a_o and b_o longitudinal acoustic sound velocities (Fig. 5). To some extent the LA sound velocities of BSN near the reentrant phase transition at $T_I' \approx 105$ K are qualitatively similar to those near the high temperature IC phase transition: c_{11} exhibits the sharper anomaly, c_{22} shows a smaller dip, and the two elastic constants gradually coalesce at a lower temperature (~95 K). There are however some important differences. The order in which these features occur is reversed with respect to temperature from that near T_I, as one might expect at a reentrant transition. More importantly, the anomalies in the Brillouin frequency shifts are much smaller near T_I' and no divergence is observed in the phonon halfwidths. It should also be pointed out that the sharp dip at 105 K in the v_{11} sound velocity was not reproducible and that the overall magnitudes of the anomalies in both v_{11} and v_{22} are not much greater than the error bars for the Brillouin frequency shifts.

The general lack of strong anomalies in the hypersonic acoustic properties of BSN near T_I' precludes a phenomenological treatment of this phase transition, such as that used to describe the IC transition at T_I.[17, 18] It is interesting however to compare the data shown in Fig. 5 with the Brillouin frequency shifts measured above room temperature by Errandonéa's group.[18] A slightly larger anisotropy is observed in our room temperature data ($\nu_{22} - \nu_{11} \sim 0.86$ GHz in our data and 0.66 GHz in that of reference 18), however the slopes at room temperature of both the ν_{11} and ν_{22} curves are nearly equal in the two sets of data. Figure 9 combines the two sets of data and shows the complete temperature dependence of the two LA phonon modes between 50 K and 673 K.

From this figure a picture emerges which describes the elastic properties of BSN over a very large temperature range. Above 582 K a tetragonal phase exists. As the temperature is lowered, competing interactions cause a soft mode to condense at the IC wavevector $\underset{\sim}{k}_I$ [Eq. (1)] resulting in a breaking of the tetragonal symmetry in the $a_t - b_t$ plane. Coupling between the IC order parameter amplitude and the shear elastic strain e_6 results in the onset of a spontaneous strain and ferroelasticity. At T_L a nearly complete lock-in occurs to a quasi-commensurate orthorhombic phase; the lack of a true commensurate phase being due to a pinning of discommensurations by point defects. The greatest elastic anisotropy $c_{22} - c_{11}$ occurs at the lock-in temperature of $\sim$ 543 K. Below this temperature there is a continuous relaxation of the elastic anisotropy primarily due to a monotonic increase in the c_{11} elastic constant between T_L and $\sim$ 110 K. Finally, a tetragonal phase exists below $\sim$ 95 K of the same exact point group symmetry as that above 582 K. The tetragonal c_{11} (or c_{22}) elastic constant continues to increase as the temperature is lowered further to 50 K (possibly 20 K), though with a slightly different slope than that above 110 K. This is most probably due to thermal contraction.

In terms of the microscopic picture there are probably competing interactions, one or more of which are temperature dependent, resulting in the observed relaxation of the elastic anisotropy in the quasi-commensurate phase. The exact nature of these microscopic interactions is at present not understood, though the role of defects is probably significant. Some evidence for critical behavior or for coupling of the LA modes to other unobserved modes also exists since the coalescence of the c_{11} and c_{22} elastic constants is accompanied by anomalies (though significantly smaller than those between 543 and 582 K). Another significant difference between the IC and reentrant transitions is the lack of anomalous behavior in the phonon halfwidths at low temperatures. This is undoubtedly related to the fact that the diffuse rods of scattered x-rays (or neutrons), found at new IC positions along b_o as the reentrant transition is approached, are never observed to condense into sharp satellites at T_I'. These phonon halfwidth and x-ray satellite observations at low temperature are in complete contrast to the behavior observed at 582 K. One possible explanation for these differences might lie in an increased dominance of interactions between the IC modulation and defects due to a smaller thermal energy at low temperatures.

There is also evidence in our new data to support the onset of a second IC phase below the reentrant phase transition. This is the observed hysteresis in the dielectric data over a large temperature region around T_I'. Very similar hysteretic effects were observed in several physical properties near the high temperature IC phase, such as the line shape of the IC x-ray satellites, the elastic constants, the dielectric constant, and the birefringence.[16, 18, 31, 46] In addition these effects are known to exist in several other IC systems.[47–49] The low temperature hysteresis in BSN is very reminescent of the thermal memory effects associated with IC phases.[50–52] Low temperature hysteretic effects similar to our dielectric observations have been observed in the birefringence.[31] Figure 10 shows a plot of our dielectric data and

the low temperature birefringence data of Schneck. Note the remarkable similarity in the temperature range over which hysteresis is observed in the two independent sets of data.

In addition to this thermal hysteresis, our dielectric data show an anomaly at $\sim$ 50 K and a reproducibility below about 30 K (i.e., no hysteresis below this point). These features suggest another phase transition somewhere in the 30 to 50 K range. In this regard our data are inconsistent with other low temperature results in BSN. Schneck and Paquet[26] reported no dielectric anomaly in this temperature region. They did however report a similar anomaly at 12 K independent of the sample studied. Several samples without the reentrant behavior near $\sim$ 100 K, as well as one with this behavior, all exhibited this 12 K anomaly. We are unable to comment on the behavior of our samples at 12 K as no measurements were made below 17 K. Just one year before the paper of Schneck and Paquet, another paper[27] first reported the reentrant transition. They measured the birefringence, the dielectric constants κ_a and κ_c, the spontaneous polarization P_S along c, and the difference in the orthorhombic lattice constants $(b_o - a_o)/a_o$ in one sample which showed the reentrant transition. It was pointed out in this paper that corrections were made in the calculation of P_S from their data due to incomplete poling. Twin domains were a problem in the low temperature Brillouin studies reported in Schneck's thesis.[31] Poling and detwinning procedures are not discussed in any of the low temperature papers. Perhaps a lack of careful detwinning and poling is responsible for the discrepancy between our data and that of the CNET group near 40 K.

Several anomalies have been observed in BSN in the low temperature data. The dielectric anomaly observed by us at $\sim$ 140 K in both κ_a and κ_b is in excellent agreement with that observed by the CNET group. This anomaly however is not at the transition temperature T_I', but rather at a higher temperature corresponding to an inflection point in the birefringence data. In addition to this inflection point,

the birefringence also shows a maximum at about 200 K. Our Brillouin data for the elastic constant c_{22} also show a maximum near 200 K followed by a continuous softening down to about 100 K. Each of these features in the low temperature data have a tendency to be sample dependent, with stoichiometry being the leading determinant for the differences among samples. Clearly more experimental studies of the low temperature properties of BSN are needed.

SUMMARY AND SUGGESTIONS FOR FURTHER WORK

We have described a number of related experiments in the sections above that involve dielectric measurements, Brillouin spectroscopy, and indices of refraction. These generally provide a self-consistent, coherent description of the low-temperature phases and characteristics of $Ba_2NaNb_5O_{15}$. However, a number of things remain to be done, which are most easily described with reference to Fig. 1b. Firstly, the space group symmetry of the lock-in phase that is stable below ca. 40 K is still uncertain: Three different space groups ($P4_2bc$, $P4nc$, and Bb) have been proposed on theoretical grounds. Second, it is uncertain whether the IC(2q) phase between 565 K and 582 K is exactly the same as that between 40 K and 105 K. Is this truly a reentrant phase (as diagrammed in Fig. 1b) with the same space group symmetry (in the four-dimensional representations of Janssen and Currat[53] for IC structures), or do the phases merely have the same average point group symmetry? Third, what is the shape of the $Ccm2_1$-IC(2q) phase boundary? Does it satisfy the free energy phenomenologic theory of Ishibashi?[54] Fourth, does the $P4bm$-IC(2q) phase boundary fit Ishibashi's theory? Finaliy, is the IC(1q)-IC(2q) phase boundary consistent with the free-energy description of Tolédano and Tolédano?[55] And does it move as one would expect with applied uniaxial stress?

As a beginning, we have recently undertaken some elastic neutron scattering experiments at LANSCE, in collaboration with P. Vergamini and A. Larson, using the single crystal diffractometer. We employed this apparatus in the belief that the structural distortions in BSN would primarily involve oxygen displacements, for which neutrons would be a more sensitive probe than x-rays. Our preliminary results, shown in Figs. 11a and b, show that the lock-in phase below 40 K does indeed involve a doubling of the primitive unit cell along both a-b diagonals of the orthorhombic cell. Figure 11a shows the Bragg scattering from the underlying tetragonal phase; Fig. 11b shows the additional Bragg peaks along the diagonals of that phase, corresponding to cell doubling along $a^* + b^*$ and $a^* - b^*$. Note the diffuse scattering that persists in both directions; this is due to residual discommensurations in the lock-in phase.

REFERENCES

1. J. E. Geusic, H. J. Levinstein, J. J. Rubin, S. Singh, and L. G. Van Uitert, Appl. Phys. Lett. **11**, 269 (1967).

2. J. E. Geusic, H. J. Levinstein, S. Singh, R. G. Smith and L. G. Van Uitert, Appl. Phys. Lett. **12**, 306 (1968).

3. L. G. Van Uitert, H. J. Levinstein, J. J. Rubin, C. D. Capio, E. F. Dearborn and W. A. Bonner, Mat. Res. Bull. **3**, 47 (1968); L. G. Van Uitert, L. G., J. J. Rubin and W. A. Bonner, IEEE J. Quant. Elec. **4**, 622 (1968).

4. W. F. Oliver, Ph.D. Thesis, University of Colorado (1988).

5. T. Yamada, H. Iwasaki, and N. Niizeki, J. Appl. Phys. **41**, 4141 (1970).

6. S. Singh, D. A. Draegert and J. E. Geusic, Phys. Rev. B **2**, 2709 (1970).

7. J. C. Tolédano, Phys. Rev. B **12**, 943 (1975).

8. J. C. Tolédano, M. Busch and J. Schneck, Ferroelectrics **13**, 327 (1976).

9. J. Burgeau and J. C. Tolédano, Solid St. Commun. **20**, 28 (1976).

10. A. Boudou and J. Sapriel, Phys. Rev. B **21**, 61 (1980).

11. J. Schneck, J. C. Tolédano, B. Joukoff, F. Denoyer and C. Joffrin, Ferroelectrics **26**, 661 (1980).

12. J. Schneck and F. Denoyer, Phys. Rev. B **23**, 383 (1980).

13. J. Schneck, J. C. Tolédano, C. Joffrin, J. Aubrée, B. Joukoff and A. Gabelotaud, Phys. Rev. B **25**, 1766 (1982).

14. J. C. Tolédano, J. C. and L. Pateau, J. Appl. Phys. **45**, 1611 (1974).

15. G. Errandonéa, J. Schneck, J. C Tolédano, A. Litzler, H. Savary, J. Aubrée, J. M. Kiat and G. Calvarin, Ferroelectrics **53**, 247 (1984).

16. J. Schneck, G. Calvarin and J. M. Kiat, Phys. Rev. B **29**, 1476 (1984).

17. P. W. Young and J. F. Scott, Ferroelectrics **52**, 35 (1983); P. W. Young and J. F. Scott, Phase Transitions **6**, 175 (1986).

18. G. Errandonéa, M. Hebbache, and F. Bonnouvrier, Phys. Rev. B **32**, 1691 (1985).

19. W. F. Oliver, J. F. Scott, S. Lee, and S. Lindsay, "Dynamic Central Modes And Photorefractive Effects At T_I and T_C In Barium Sodium Niobate," in *Laser Optics Of Condensed Matter*, ed. by J. L. Birman, H. Z. Cummins, and A. A. Kaplyanskii (Plenum, New York, 1988), p. 263.

20. W. F. Oliver, J. F. Scott, S. A. Lee, and S. M. Lindsay, to appear in Materials Letters.

21. P. B. Jamieson, S. C. Abrahams and J. L.Berstein (1969), J. Chem. Phys. 50, 4352 (1969).

22. P. Xiao-qing, H. Mei-shen, Y. Ming-hui, and Feng Duan, Phys. Stat. Sol. **91**, 57 (1985).

23. G. Van Tendeloo, S. Amelinckx, C. Manolikas, and W. Shulin, Phys. Stat. Sol. **91**, 483 (1985).

24. C. Manolikas, J. Schneck, J. C. Tolédano, J. M. Kiat, and G. Calvarin, Phys. Rev. B **35**, 8884 (1987).

25. J. C. Tolédano, J. Schneck, G. Errandonéa, R. Currat and D. Petitgrand, Proc. 2nd Int'l. conf. on Phonon Physics, Budapest, Hungary (World Press, 1985), p. 290.

26. J. Schneck and D. Paquet, Ferroelectrics **21**, 577 (1978).

27. J. Schneck, J. Primot, R. von der Mühll and J. Ravez, Solid St. Commun. **21**, 57 (1977).

28. M. E. Lines and A. M. Glass, *Principles and Applications of Ferroelectrics and Related Materials*, (Oxford University Press, Oxford, 1977), p. 347.

29. R. T. Harley, W. Hayes, A. M. Perry, S. R. P. Smith, R. J. Elliot and I. D. Seville, J. Phys. C.: Solid State **7**, 3145 (1974).

30. J. Schneck, B. Joukoff and R. Mellet, Ferroelectrics **26**, 775 (1980).

31. Jacques Schneck, Ph.D. Thesis, University of Paris VI (1982).

32. A. Yoshihara, E. R. Bernstein, and J. C. Raich, J. Chem. Phys. **77**, 2768 (1982).

33. R. Vacher and L. Boyer, Phys. Rev. B **6**, 639 (1972).

34. H. Z. Cummins and P. E. Schoen, "Absolute Cross Sections for Raman and Brillouin Scattering," in the *Laser Handbook*, Vol. 2, ed. by F. T. Arrechi and E. O. Schultz-Dubois (North-Holland, Amsterdam, 1972), p. 1029.

35. Amnon Yariv, *Optical Electronics*, 2nd ed. (Holt, Rinehart and Winston, New York, 1976), p. 62.

36. P. R. Bevington, *Data Reduction And Error Analysis for the Physical Sciences* (McGraw-Hill, New York, 1969), ch. 11.

37. W. E. Wentworth, J. Chem. Educ. **42**, 96 (1965).

38. S. M. Lindsay, S. Burgess and I. W. Shepherd, Appl. Optics **16**, 1404 (1977).

39. G. B. Benedek and K. Fritsch, Phys. Rev. **149**, 647 (1966).

40. J. F. Nye, *Physical Properties of Crystals*, (Clarendon Press, Oxford, 1985).

41. A. Ashkin, G. D. Boyd, J. M. Dziedzic, R. G. Smith, A. A. Ballman, J. J. Levinstein and K. Nassau, Appl. Phys. Lett. **9**, 72 (1966).

42. F. S. Chen, J. Appl. Phys. **40**, 3389 (1969).

43. A. M. Glass and M. E. Lines, Phys. Rev. B. **13**, 180 (1976).

44. S. G. Odulov, JETP Lett. **1**, 10 (1982); S. G. Odulov and O. I. Oleĭnik, Sov. Phys. Solid State **27**, 2093 (1985).

45. W. F. Oliver and J. F. Scott, "Thermal Memory and Phase Conjugation Experiments in Incommensurate Barium Sodium Niobate," in *Incommensurate Crystals, Liquid Crystals, and Quasi-crystals*, ed. by J. F. Scott and N. A. Clark, (Plenum, New York, 1987), p. 177.

46. G. Errandonéa, J. C. Tolédano, A. Litzler, H. Savary, J. Schneck, and J. Aubrée, J. Physique Lett. **45**, L329 (1984).

47. A. H. Moudden, F. Denoyer, M. Lambert, and W. Fitzgerald, Solid St. Commun. **32**, 933 (1979).

48. K. Hamano, T. Hishinuna, and K. Ema, J. Phys. Soc. Japan **50**, 2666 (1981).

49. H. Mashiyama, S. Tanisaki, and K. Hamano, J. Phys. Soc. Japan **51**, 2538 (1982).

50. J. P. Jamet and P. Lederer, J. Physique Lett. **44**, L257 (1983).

51. P. Lederer, G. Montambaux, J. P. Jamet, and M. Chauvin, J. Physique Lett. **45**, L627 (1984).

52. H. G. Unruh, J. Phys. C: Solid State **16**, 3245 (1983).

53. T. Janssen and R. Currat, "Elastic Scattering From Quasi-periodic Structures," in *Incommensurate Crystals, Liquid Crystals, and Quasi-crystals*, ed. by J. F. Scott and N. A. Clark (Plenum, New York, 1987), p. 19.

54. Y. Ishibashi, "A Phenomenological Theory of the Transition Sequence Including an Incommensurate (Commensurate) Phase Sandwiched by a Reentrant Commensurate (Incommensurate) Phase," in *Incommensurate Crystals, Liquid Crystals, and Quasi-crystals*, ed. by J. F. Scott and N. A. Clark (Plenum, New York, 1987), p. 1.

55. J. C. Tolédano and P. Tolédano, *The Landau Theory of Phase Transitions*, (World Scientific, Singapore, 1987), sec. 2.

FIGURE CAPTIONS

Figure 1: a) Phase transition temperatures, lattice constants, and point-group symmetries of the different phases of BSN as understood at the beginning of this work. At 838 K BSN undergoes a phase transition from a paraelectric (PE) to a ferroelectric (FE) phase of tetragonal symmetry. An incommensurate (IC) transition to a ferroelastic (Fe) phase with an IC modulation wavevector $\underset{\sim}{k}_I$ occurs at 582 K, followed by a nearly complete lockin transition at 543 K to a quasi-commensurate (QC) phase of orthorhombic symmetry. This phase reverts back to a tetragonal phase near 105 K through another IC transition. Evidence also exist for yet another transition at lower temperatures. b) Schematic phase diagram, showing pressure versus temperature, for $Ba_2NaNb_5O_{15}$. The phase boundaries for $P > 0$ are largely hypothetical, although the $Ccm2_1$ to IC(2q) boundary has some data points (marked by x's) obtained via a hot-stage optical microscopy experiment [S. Kojima, K. Asaumi, T. Nakamura, and S. Minomura, J. Phys. Soc. Jpn. **45**, 1433 (1978)]. The exact shape of this $Ccm2_1$-IC(2q) phase boundary (which is reentrant upon cooling and therefore unusual) may be calculated from the phenomenological free energy expression of Y. Ishibashi (*Incommensurate Crystals, Liquid Crystals, and Quasi-crystals*, ed. by J. F. Scott and N. A. Clark Plenum Press, New York, 1987, p. 1), with one adjustable parameter; similarly, the *P4bm*-IC(2q) phase boundary near 600 K may be calculated from the same theory, with a second adjustable parameter. In addition, the IC(1q)-IC(2q) phase boundary can be calculated from a (different) free energy given by J. C. Tolédano and P. Tolédano (in *The Landau Theory of Phase Transitions*, World Scientific Publishing Co., Singapore, 1987, section 2). The width of the IC(1q) phase can be increased by the application of uniaxial stress until it reaches the $P = 0$ *P4bm* commensurate phase at 582 K; see P. Bastie, F. Mogeon, and C. M. E. Zeyen, Phys. Rev. B **37**, 786 (1988).

Figure 2: Schematic diagram of the Brillouin optical, data acquisition, and stabilization systems used in the low temperature light scattering experiments.

Figure 3: Brillouin spectrum of BSN taken at 296 K showing both the LA and TA modes. A FSR of 31.70 GHz was used to record this spectrum. The LA mode on the right is assigned to the Rayleigh line one order to the left of zero frequency shift, and the TA mode on the right is assigned to the Rayleigh line at zero frequency shift.

Figure 4: Brillouin spectrum of BSN taken at 95 K in the low temperature tetragonal phase. Both the FSR and the mode assignments are the same as those in Fig. 3.

Figure 5: Temperature dependences of the pure LA and TA phonon modes along the orthorhombic a_o (γ_1 and γ_3) and b_o (γ_4 and γ_5) directions. Data from two different runs are shown for $q|||[100]_o$ and from three different runs for $q|||[010]_o$. Sample II was used for these measurements.

Figure 6: Low temperature behavior of the quasi-LA (γ_{10}) and quasi-TA (γ_{12}) modes in BSN. Again data from different runs are indicated by the two different symbols. Sample I was used for these measurements.

Figure 7: Temperature dependences of the dielectric constants κ_a and κ_b (referred to the orthorhombic axes). Measurements were made at 120 kHz. The orthorhombic anisotropy disappears at $\sim$ 130 K; however, the two dielectric constants differ in value between $\sim$ 40 K and $\sim$ 130 K. All of the data shown here were obtained on cooling runs.

Figure 8: Typical hysteresis curve for the dielectric κ_a measured at 120 kHz. A similar hysteresis was also observed for κ_b.

Figure 9: Temperature dependences of the LA mode frequencies from 20 K to 673 K. The data below room temperature is ours, and that above is from G. Errandonéa, M. Hebbache, and F. Bonnouvrier, Phys. Rev. B **32**, 1691 (1985). Squares represent the LA mode for $q|||[100]$ and circles the LA mode for $q|||[010]$, referred to the orthorhombic axes.

Figure 10: Dielectric data from this work and birefringence data from the Ph. D. thesis of J. Schneck, University of Paris VI (1982). Hysteresis is observed in both sets of data over nearly the same temperature range. Arrows indicate the direction of heating (or cooling) in the birefringence data.

Figure 11: a) (0 0 10) Bragg scattering in $Ba_2NaNb_5O_{15}$ at 10 K, showing the underlying tetragonal structure; b) (0 0 7) Bragg scattering at the same temperature. Here (for odd-L) the underlying Bragg peaks are symmetry forbidden, and the additional Bragg peaks are due to the cell-doubling transition at ca. 40 K, with doubling along $a^* + b^*$ and $a^* - b^*$. A complete refinement of the structure is in process, which at present favors the $P4nc$ space group.

Fig. 1

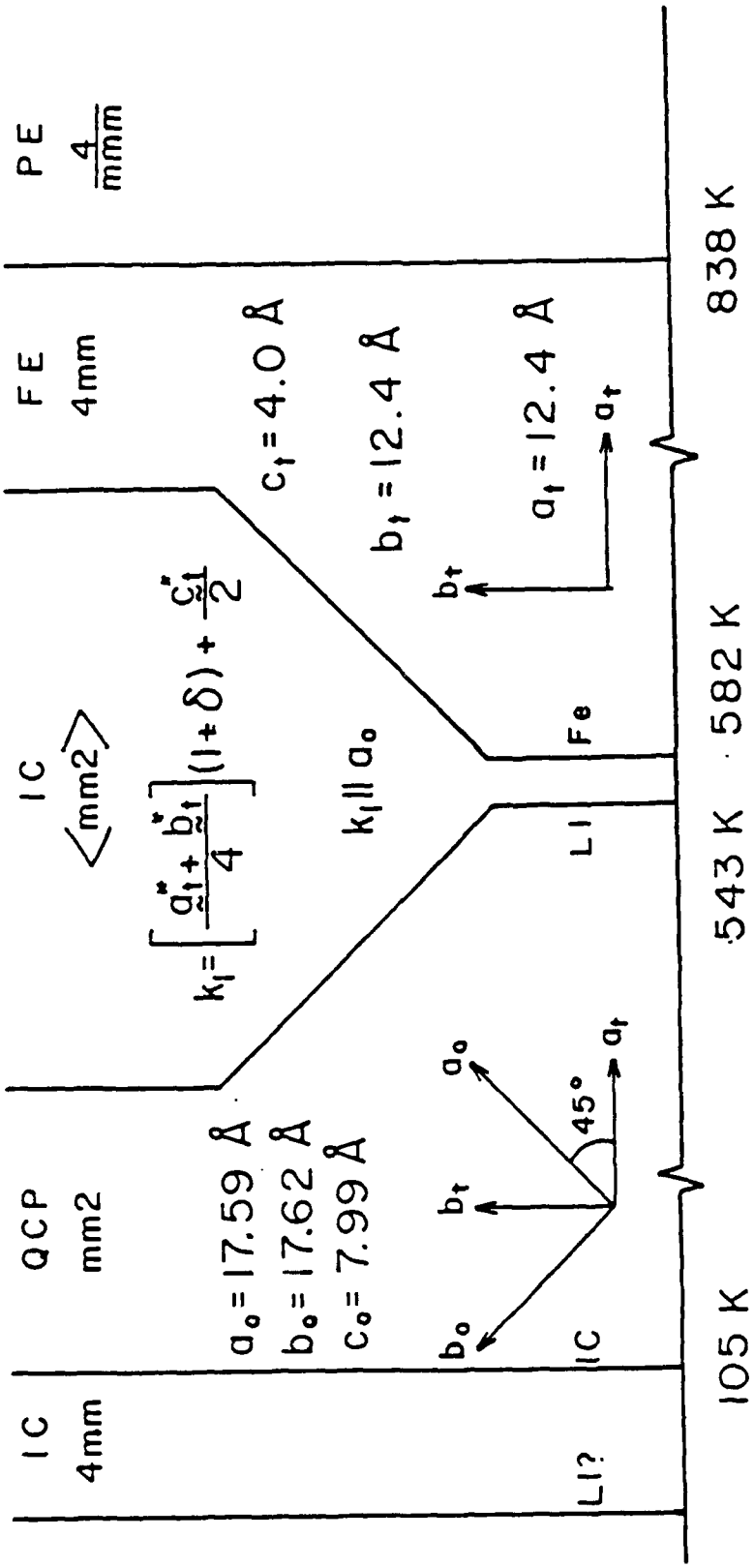
PE
4/mmm
FE
4mm
IC
<mm2>
QCP
mm2
IC
4mm
838 K
582 K
543 K
105 K
$k_1 = \left[\frac{a_1^* + b_1^*}{4}\right](1+\delta) + \frac{c_1^*}{2}$
$k_1 \| a_0$
$c_t = 4.0$ Å
$b_t = 12.4$ Å
$a_t = 12.4$ Å
a_t
b_t
Fe
L1
a_0
b_t
45°
a_t
b_0
IC
L1?
$a_0 = 17.59$ Å
$b_0 = 17.62$ Å
$c_0 = 7.99$ Å

Fig 1b

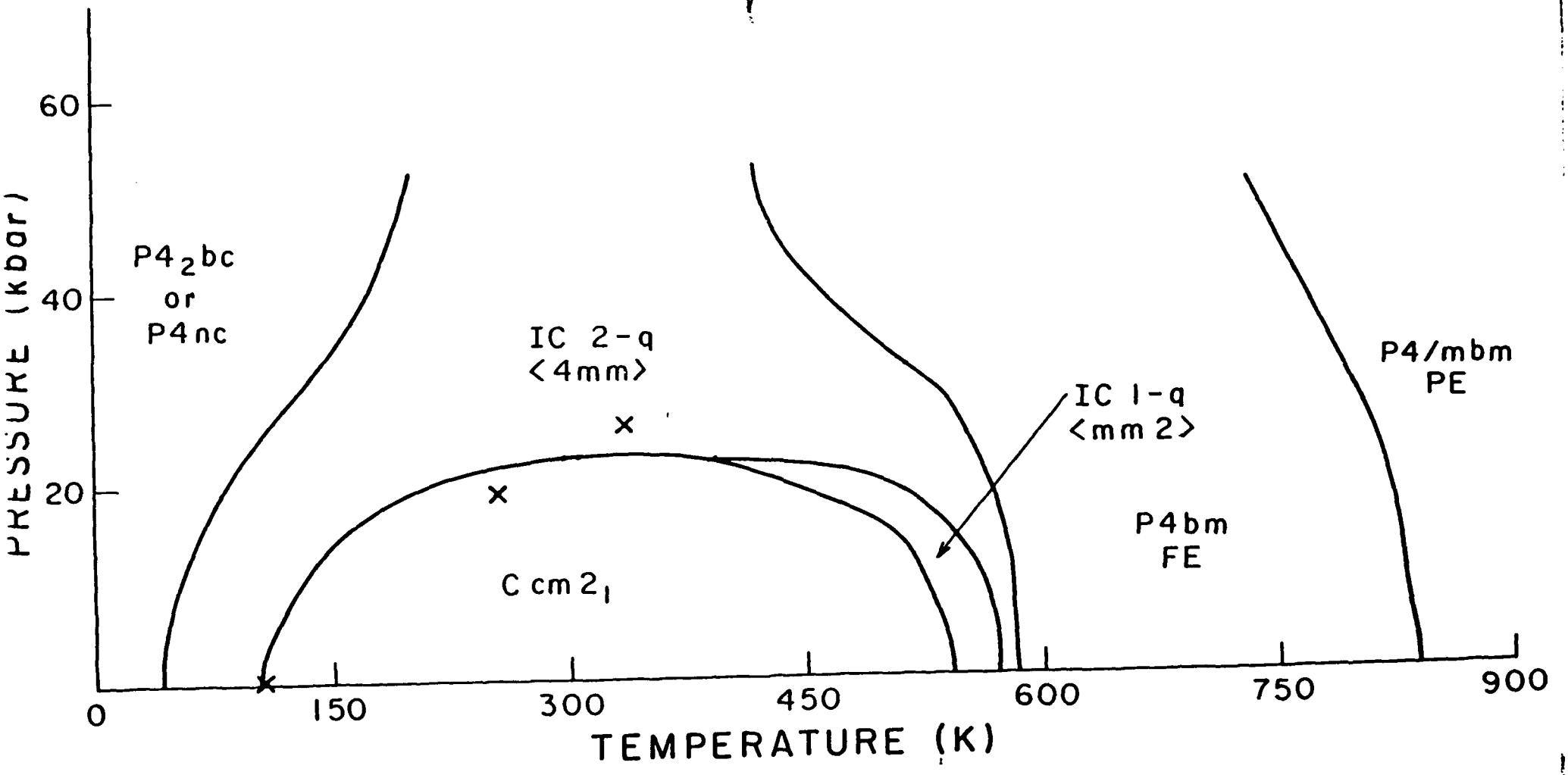
60
40
20
PRESSURE (kbar)
P4$_2$bc
or
P4nc
IC 2-q
<4mm>
IC 1-q
<mm2>
P4/mbm
PE
P4bm
FE
C cm2$_1$
0
150
300
450
600
750
900
TEMPERATURE (K)

Fig. 2

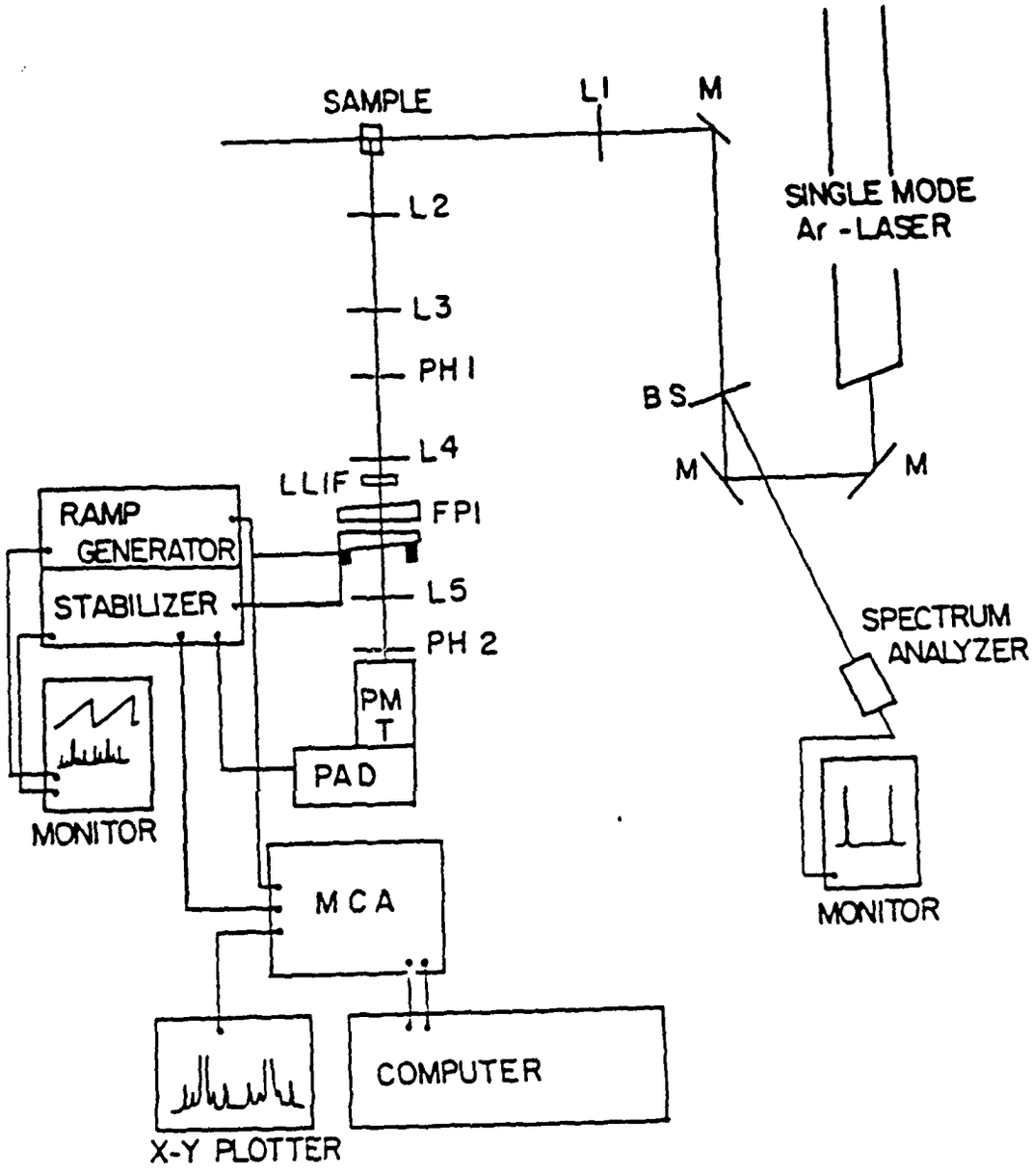
SAMPLE
L1
M
SINGLE MODE
Ar - LASER
L2
L3
PH 1
BS
L4
M
M
LLIF
FPI
RAMP
GENERATOR
STABILIZER
L5
PH 2
SPECTRUM
ANALYZER
PM
T
PAD
MONITOR
MONITOR
MCA
COMPUTER
X-Y PLOTTER

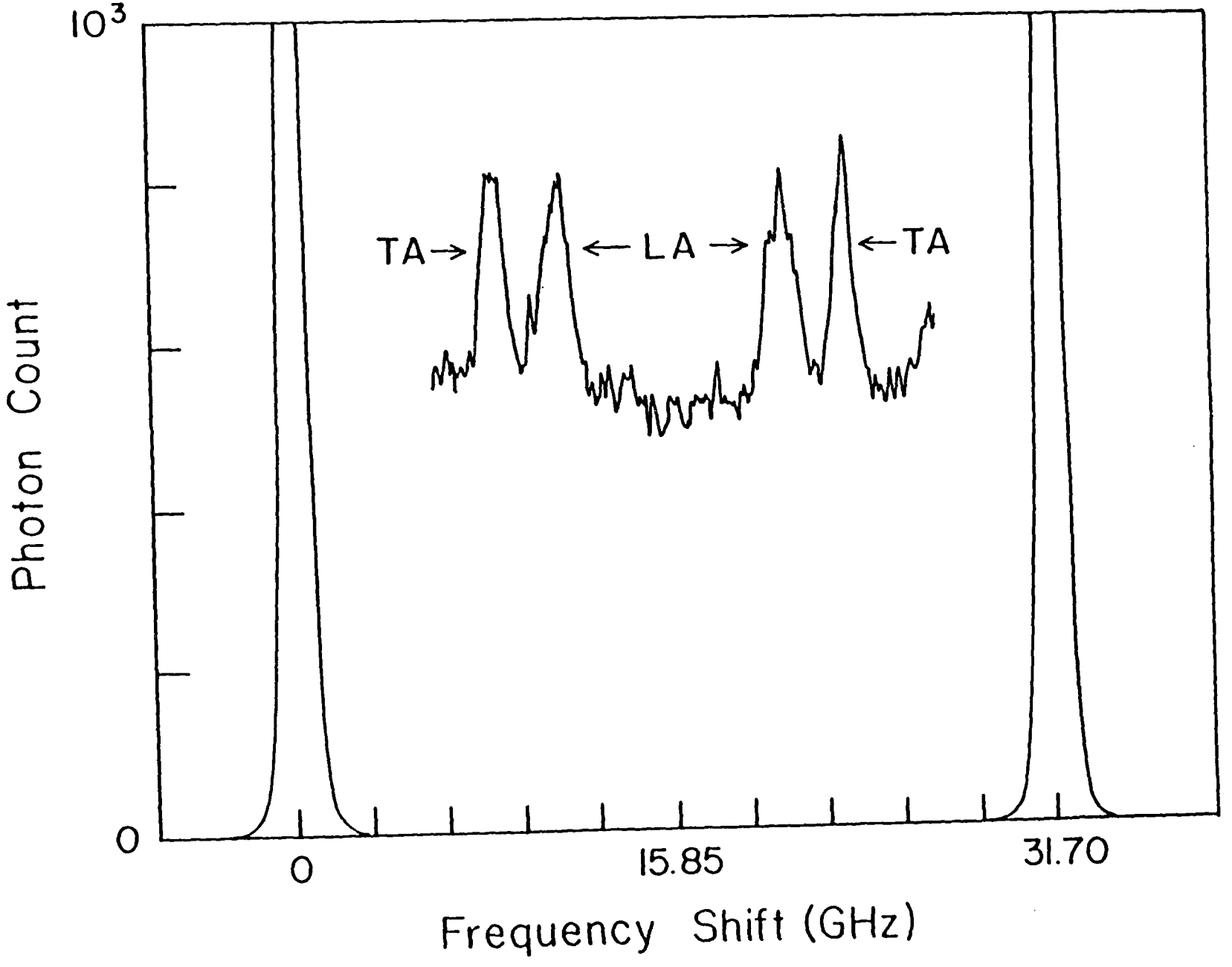

Fig. 3

Fig. 4

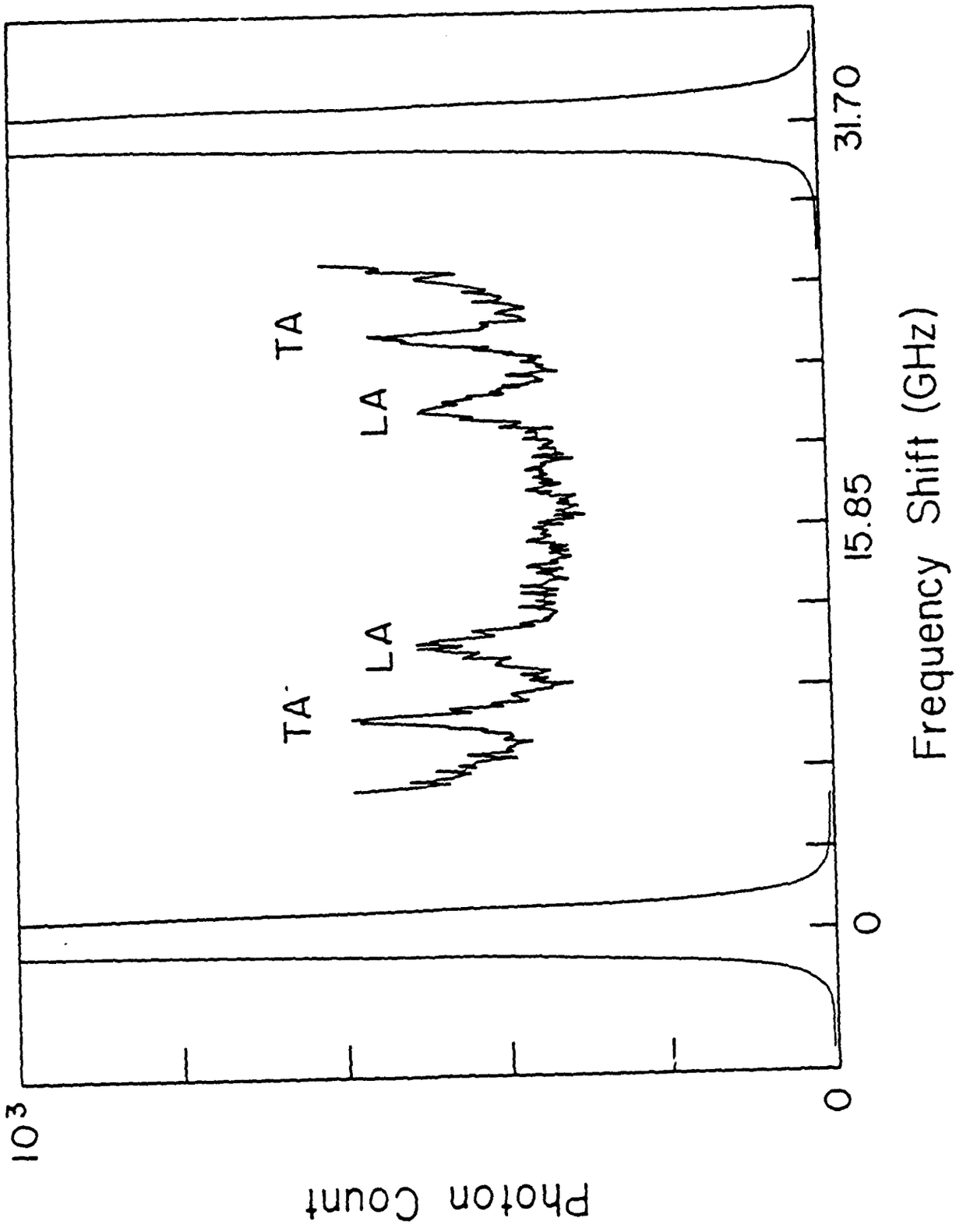

Fig. 5

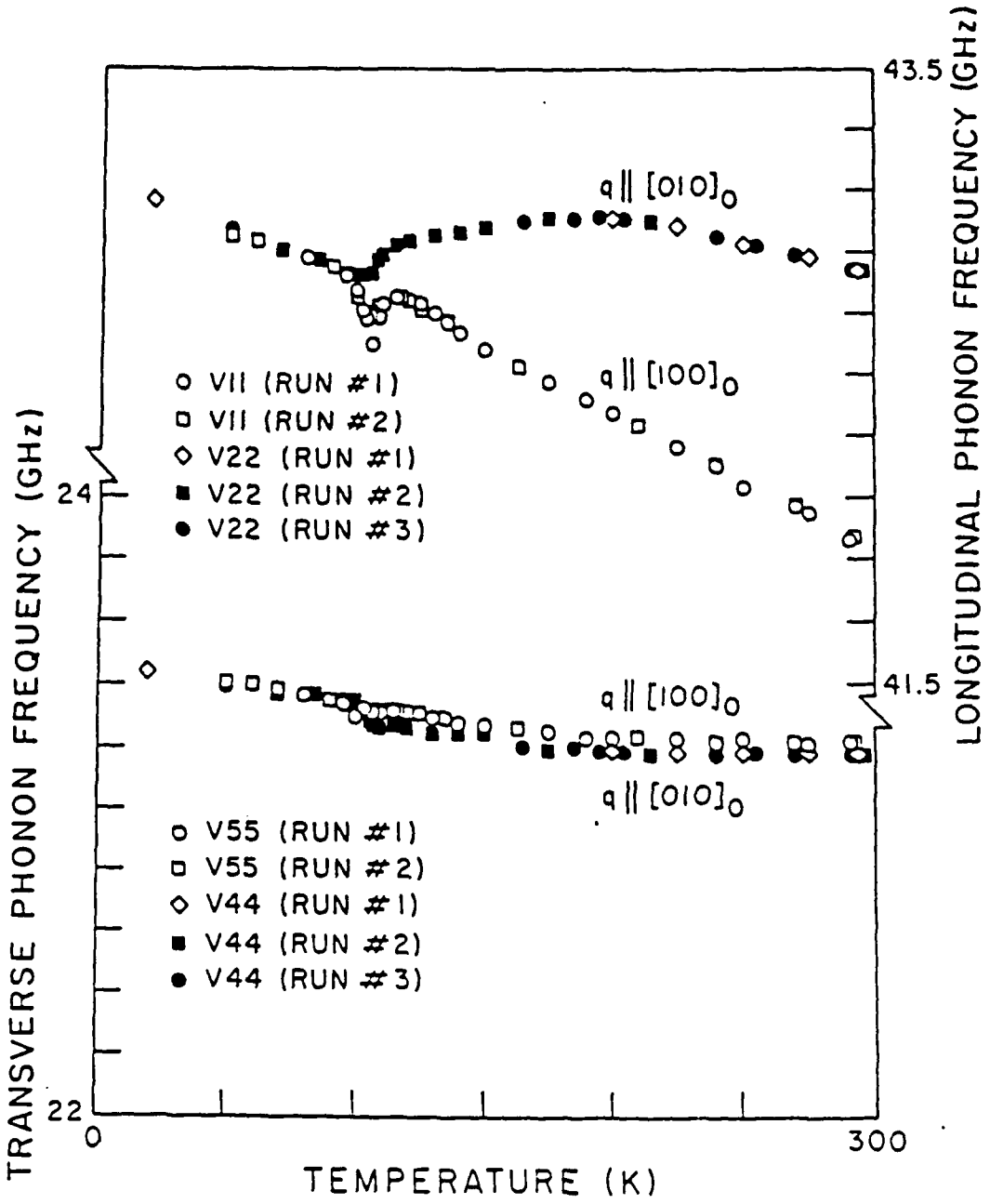
TRANSVERSE PHONON FREQUENCY (GHz)
LONGITUDINAL PHONON FREQUENCY (GHz)
TEMPERATURE (K)
24
22
43.5
41.5
0
300
q ∥ [010]₀
q ∥ [100]₀
q ∥ [100]₀
q ∥ [010]₀
V11 (RUN #1)
V11 (RUN #2)
V22 (RUN #1)
V22 (RUN #2)
V22 (RUN #3)
V55 (RUN #1)
V55 (RUN #2)
V44 (RUN #1)
V44 (RUN #2)
V44 (RUN #3)

Fig. 6

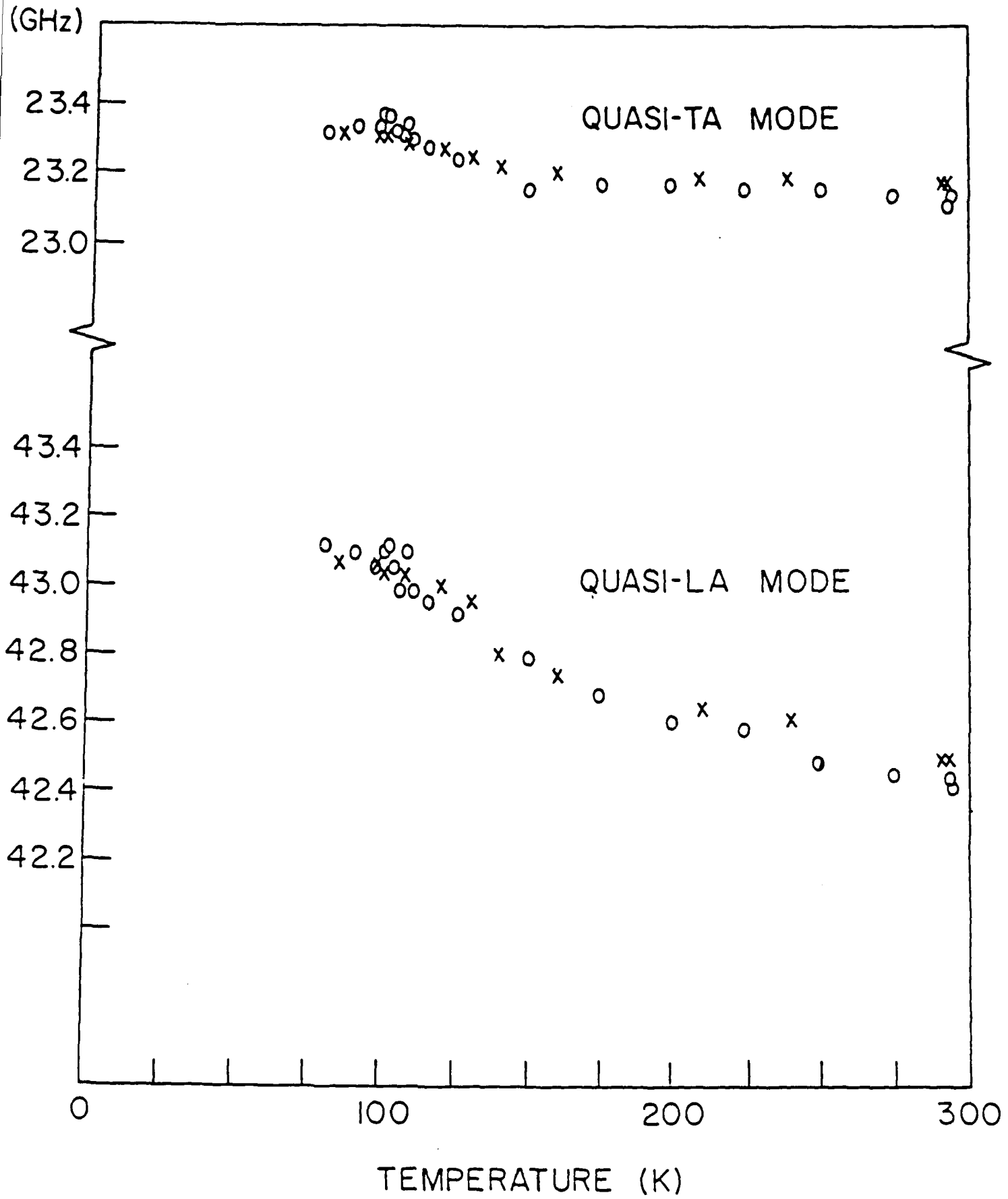
(GHz)
23.4
23.2
23.0
QUASI-TA MODE
43.4
43.2
43.0
42.8
42.6
42.4
42.2
QUASI-LA MODE
0
100
200
300
TEMPERATURE (K)

Fig. 7

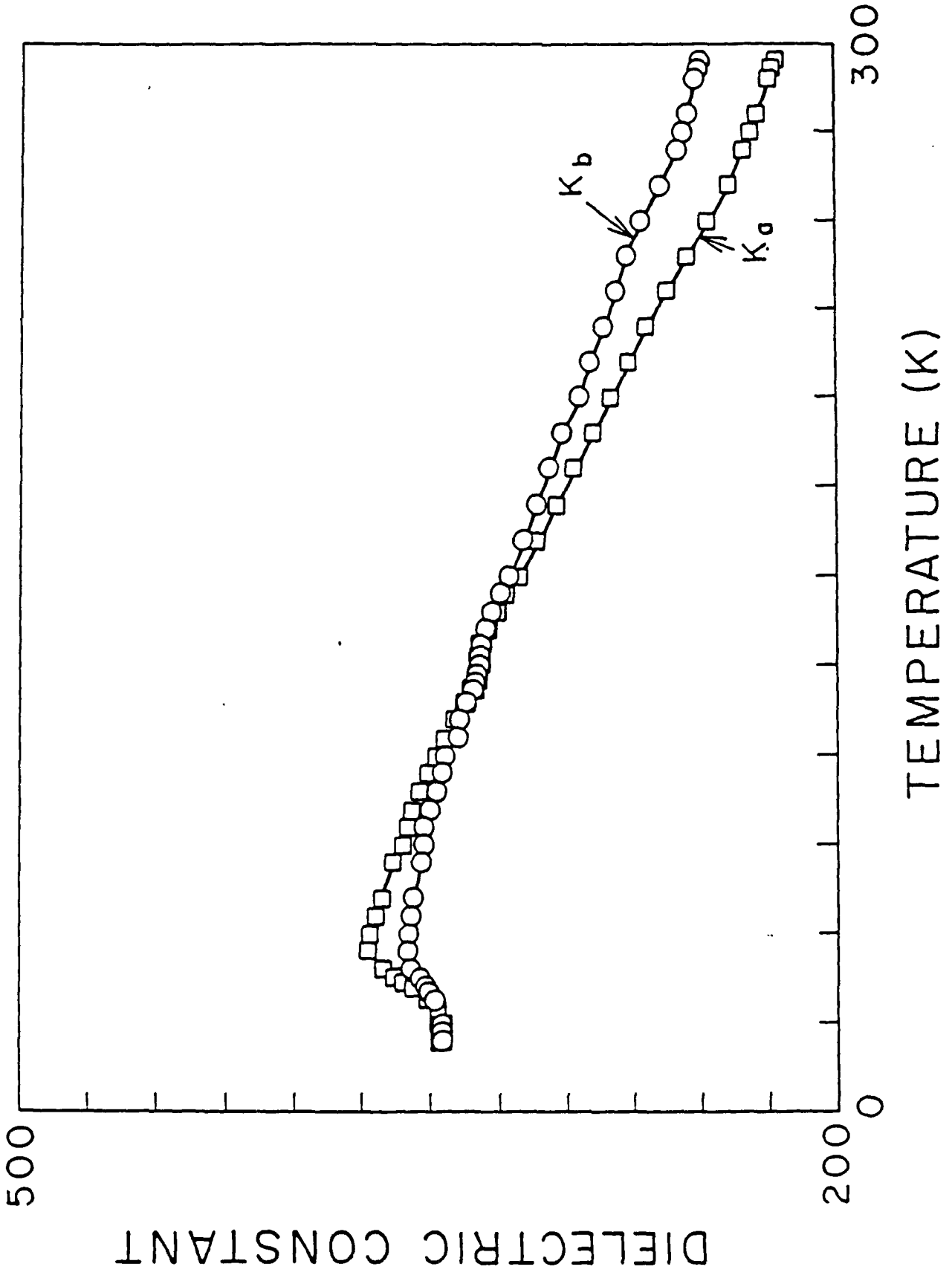

Fig. 5

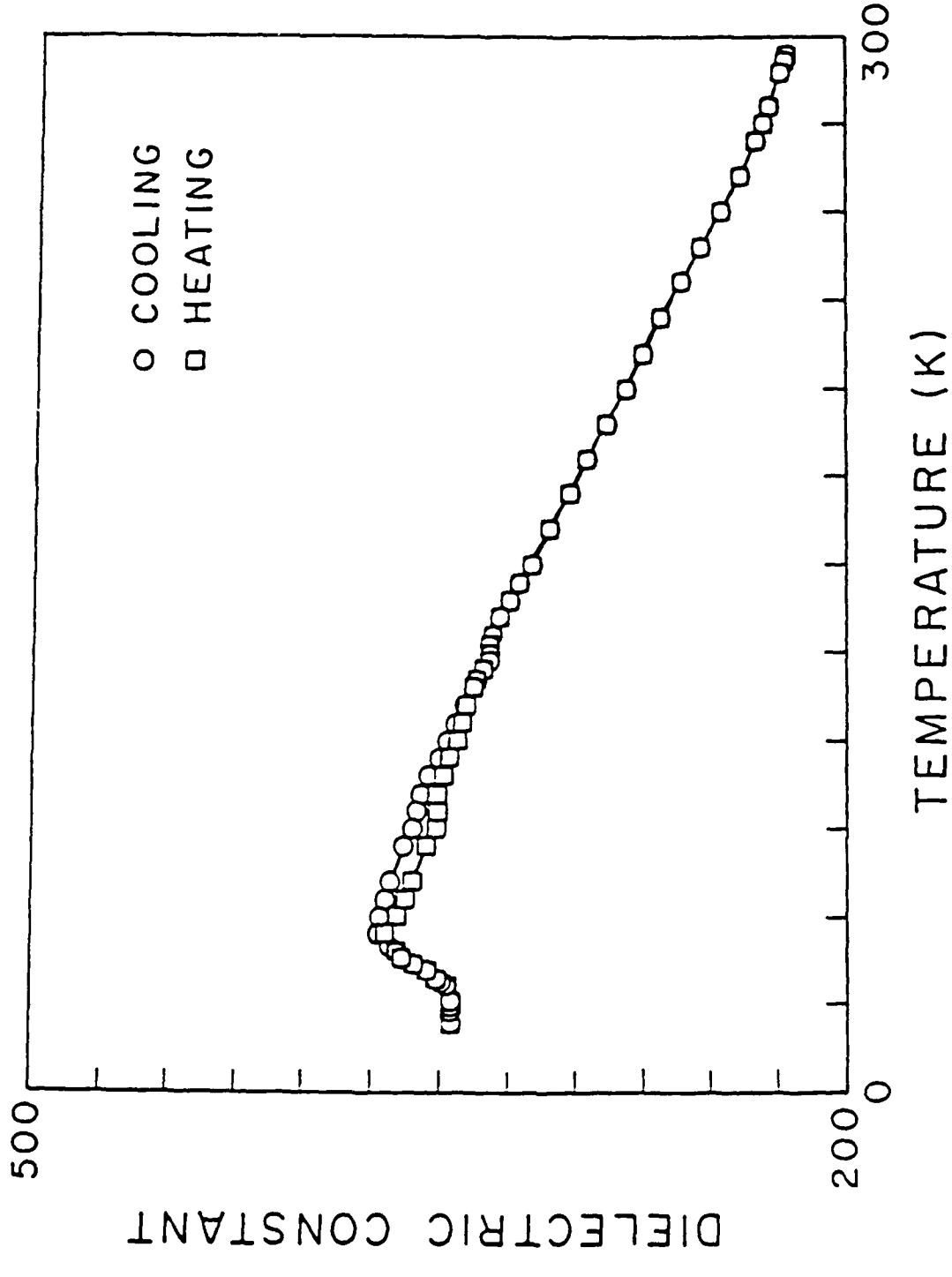
DIELECTRIC CONSTANT
500
200
0
300
TEMPERATURE (K)
O COOLING
□ HEATING

Fig. 9

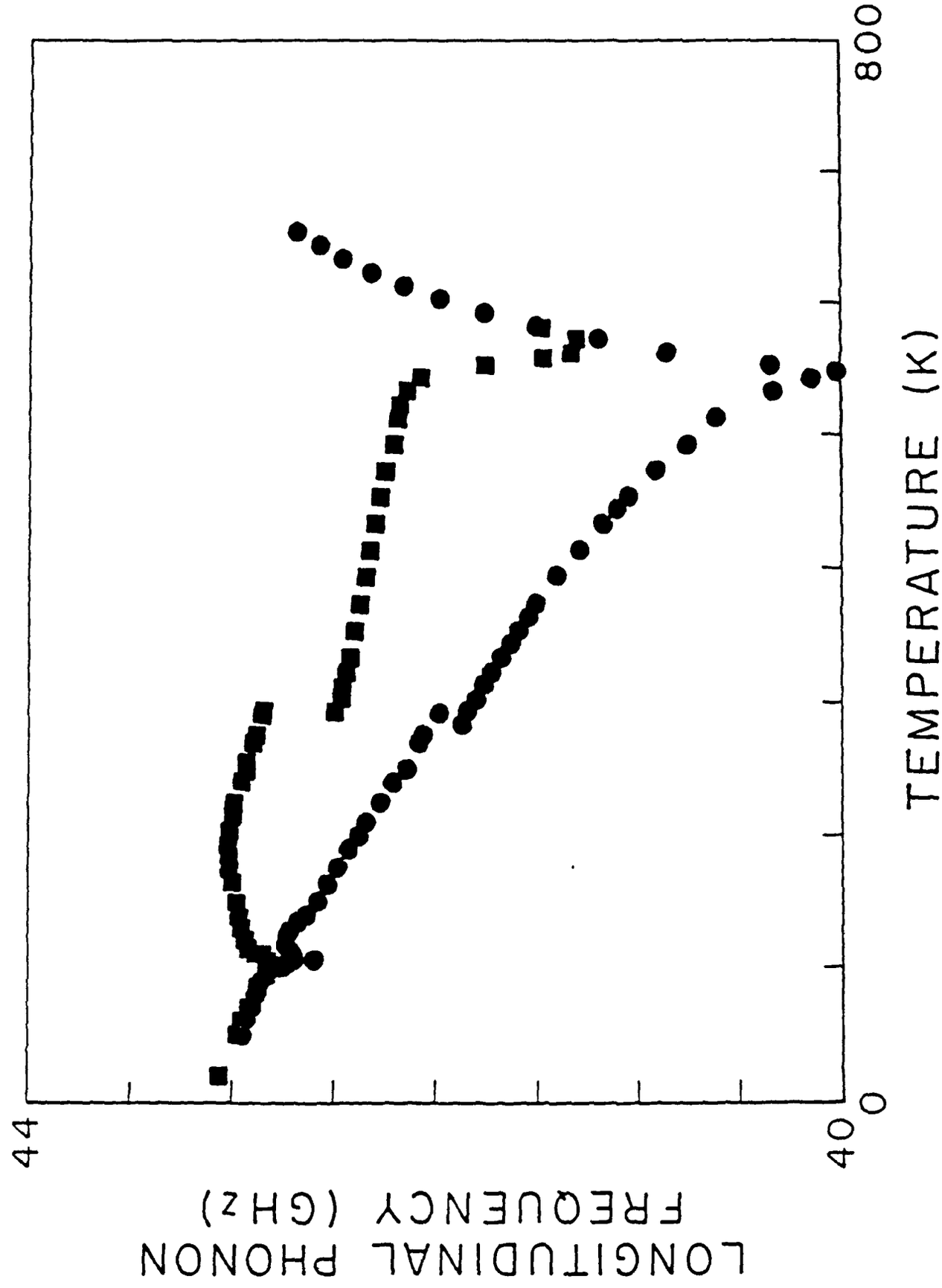
LONGITUDINAL PHONON
FREQUENCY (GHz)
44
40
0
800
TEMPERATURE (K)

Fig. 1c

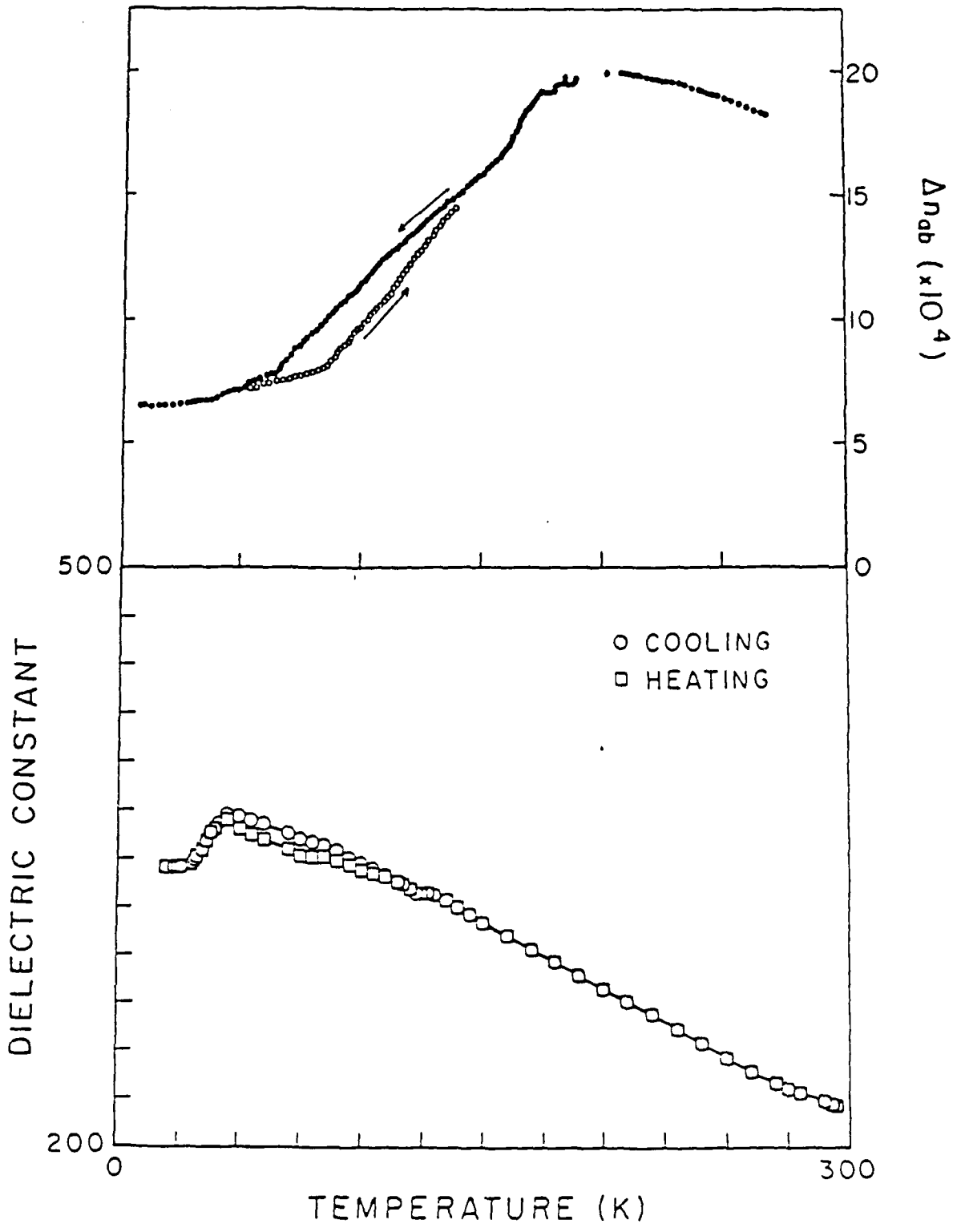
20
15
10
5
0
Δn_{ab} ($\times 10^4$)
500
200
0
300
DIELECTRIC CONSTANT
TEMPERATURE (K)
COOLING
HEATING

11a

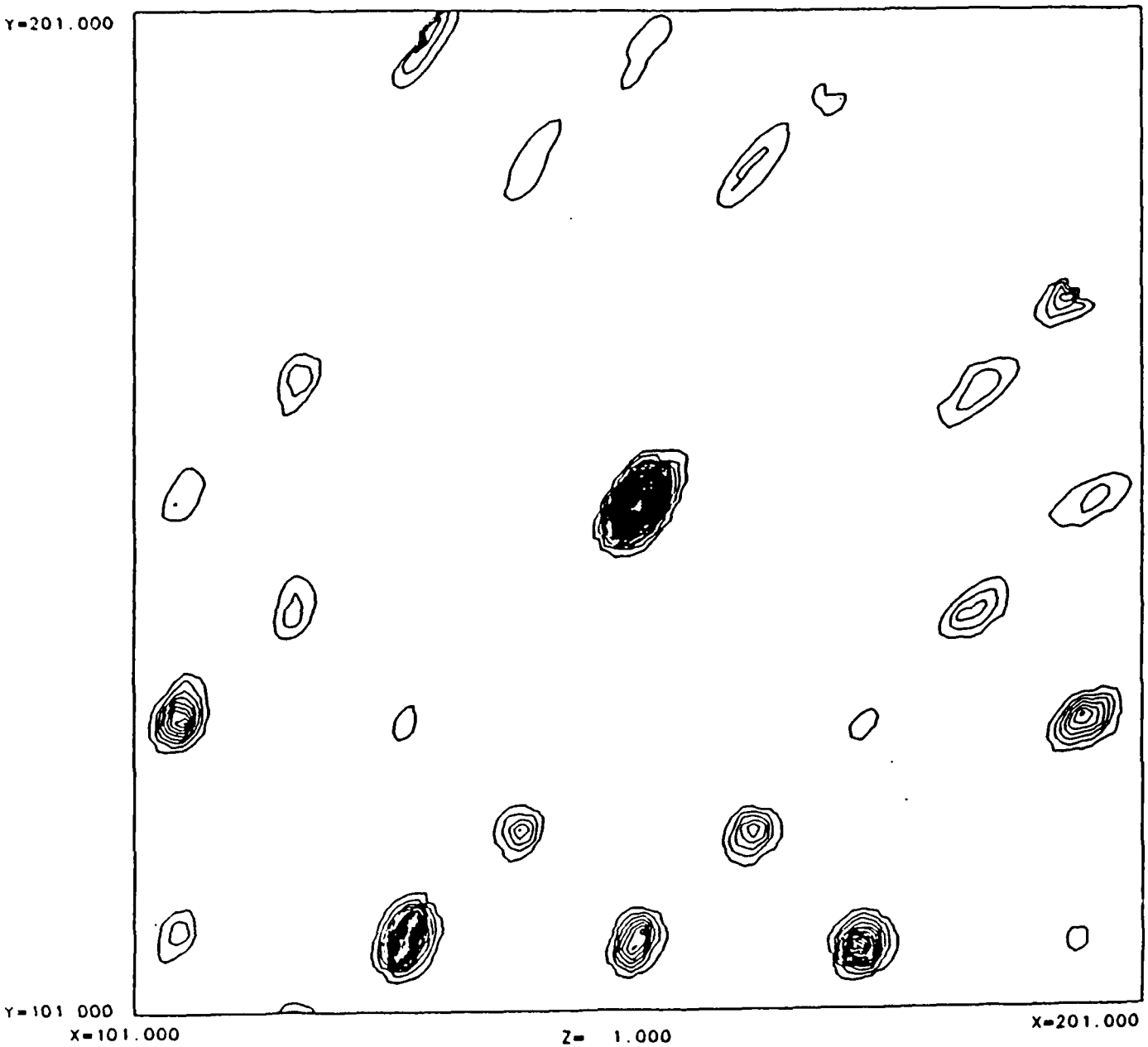

BANANAS HISTOGRAM 1 CENTER= 0.0 0.0 10.0 GRID=0.005

A2NANB5015 AT 10K HORZ 1.0 0.0 0.0 VERT 0.0 1.0 0.0

HE RANGE OF RHO VALUES IS FROM 0.000E+00 TO 2.474E+03

ATE = 21-JUL-88 TIME = 12 51 40 CONTOUR INTERVAL = 10.0

(11b)

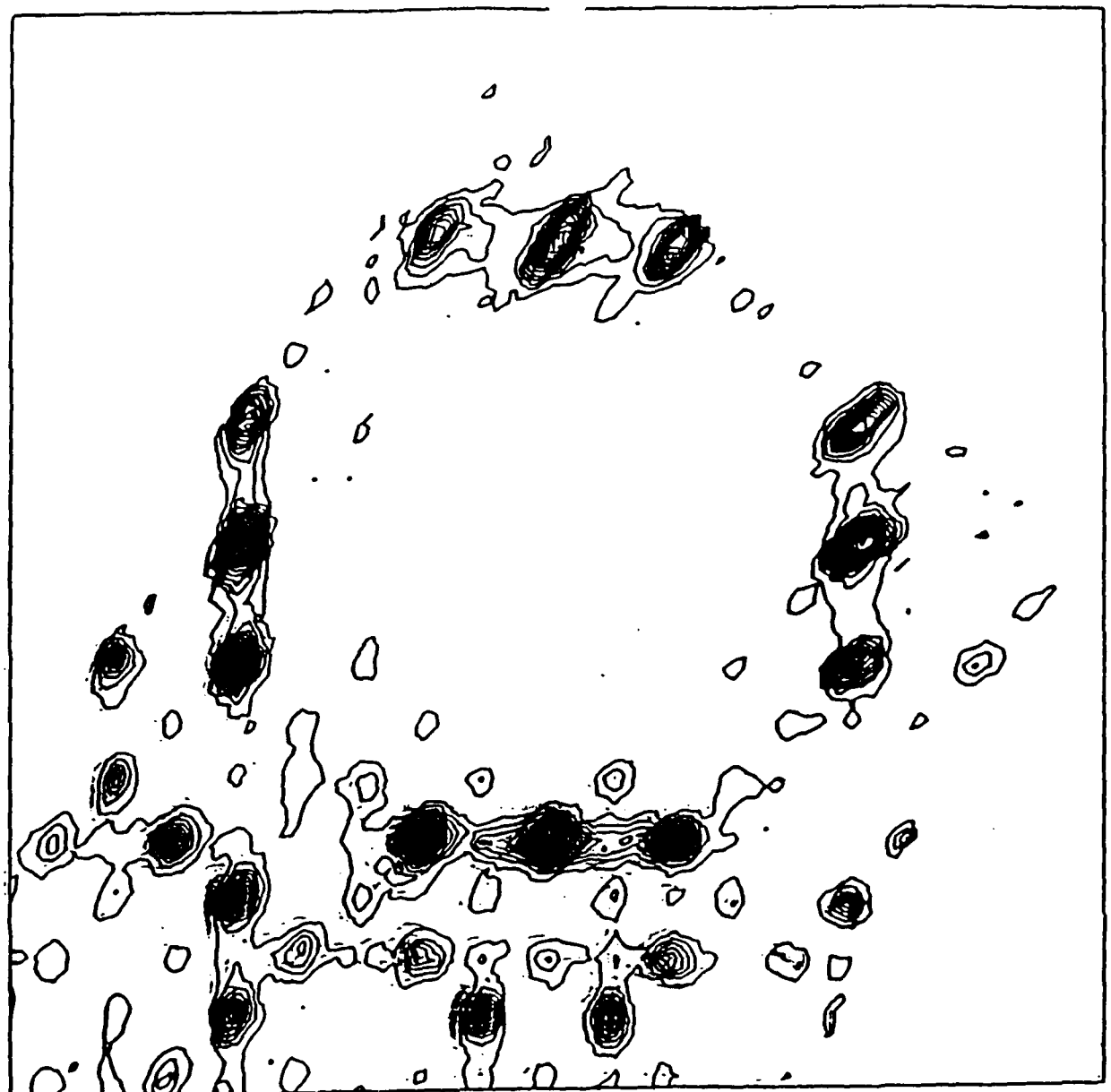

ANANAS HISTOGRAM 1 CENTER= 0.0 0.0 7.0 GRID=0.005

2NAND3015 AT 10K HORZ 1.0 0.0 0.0 VERT 0.0 1.0 0.0

E RANGE OF RHO VALUES IS FROM 0.000E+00 TO 2.474E+03

TE = 21-JUL-88 TIME = 12 40 13 CONTOUR INTERVAL = 5.00

TABLE CAPTIONS

Table 1: Scattering geometries for the observed acoustic modes in the reference frame of the $\underset{\sim}{a}_o$, $\underset{\sim}{b}_o$, $\underset{\sim}{c}_o$ orthorhombic axes. The first column gives the sample number. In the next four columns the directions of the incident and scattered beams and their respective polarizations are given. Next the phonon propagation direction is given, followed by the phonon polarization (Pol.: QLA and QTA referring to quasi-LA and quasi-TA, respectively. Finally, a mode label is given [following the notation of R. Vacher and L. Boyer, Phys. Rev. B 6, 639 (1972)].

Table 2: Expressions for ρv^2 in terms of the elastic constants for the different observed acoustic modes. Piezoelectric corrections to the elastic constants have been left out [see R. Vacher and L. Boyer, Phys. Rev. B 6, 639 (1972)].

Table 1

Sample	$\underset{\sim}{k}_i$	$\underset{\sim}{k}_s$	$\hat{e}_i$	$\hat{e}_s$	q	Pol.	Observed Mode
I	[$\bar{1}$00]	[010]	[001]	[001]	[110]	QL	γ_{10}
				[100]		QT	γ_{12}
II	[110]	[$\bar{1}$10]	[001]	[001]	[100]	L	γ_1
				[110]		T	γ_3
II	[1$\bar{1}$0]	[110]	[001]	[001]	[010]	L	γ_4
				[1$\bar{1}$0]		T	γ_5

Table 2

Mode	ρv^2 Orthorhombic Phase	ρv^2 Tetragonal Phase
γ_1	c_{11}	c_{11}
γ_3	c_{55}	c_{44}
γ_4	c_{22}	c_{11}
γ_5	c_{44}	c_{44}
γ_{10}	$\frac{1}{4}\{c_{11}+c_{22}+2c_{66}$ $+[(c_{11}-c_{22})^2+4(c_{12}+c_{66})^2]^{1/2}\}$	$(c_{11}+c_{12})/2+c_{66}$
γ_{12}	$\frac{1}{2}(c_{44}+c_{55})$	c_{44}

DL/1113/89/1

TECHNICAL REPORT DISTRIBUTION LIST, GENERAL

	No. Copies
Office of Naval Research Chemistry Division, Code 1113 800 North Quincy Street Arlington, VA 22217-5000	3
Commanding Officer Naval Weapons Support Center Attn: Dr. Bernard E. Douda Crane, IN 47522-5050	1
Dr. Richard W. Drisko Naval Civil Engineering Laboratory Code L52 Port Hueneme, California 93043	1
Defense Technical Information Center Building 5, Cameron Station Alexandria, Virginia 22314	2 high quality
David Taylor Research Center Dr. Eugene C. Fischer Annapolis, MD 21402-5067	1
Dr. James S. Murday Chemistry Division, Code 6100 Naval Research Laboratory Washington, D.C. 20375-5000	1
Dr. Ronald L. Atkins Chemistry Division (Code 385) Naval Weapons Center China Lake, CA 93555-6001	1
Chief of Naval Research Special Assistant for Marine Corps Matters Code 00MC 800 North Quincy Street Arlington, VA 22217-5000	1
Dr. Bernadette Eichinger Naval Ship Systems Engineering Station Code 053 Philadelphia Naval Base Philadelphia, PA 19112	1
Dr. Sachio Yamamoto Naval Ocean Systems Center Code 52 San Diego, CA 92152-5000	1
David Taylor Research Center Dr. Harold H. Singerman Annapolis, MD 21402-5067 ATTN: Code 283	1